



An insight into long-term continuity in global land surface phenology: A comparative analysis of MODIS and VIIRS products



Khuong H. Tran^{a,b,c,*}, Xiaoyang Zhang^{a,*}, Yongchang Ye^a, Geoffrey M. Henebry^{d,e}, Mark A. Friedl^f, Yu Shen^{a,g}, Yuxia Liu^a, Shuai An^a, Shuai Gao^a

^a Geospatial Sciences Center of Excellence, Department of Geography and Geospatial Sciences, South Dakota State University, Brookings, SD 57007, USA

^b NASA Ames Research Center, Moffett Field, CA 94035, USA

^c Bay Area Environmental Research Institute, Moffett Field, CA 94035, USA

^d Department of Geography, Environment, and Spatial Sciences, Michigan State University, East Lansing, MI 48824, USA

^e Center for Global Change and Earth Observations, Michigan State University, East Lansing, MI 48823, USA

^f Department of Earth and Environment, Boston University, MA 02215, USA

^g Nicholas School of the Environment, Duke University, Durham, NC 27708, USA

ARTICLE INFO

Keywords:

Land surface phenology

Land cover dynamics

MODIS

VIIRS

Continuity

Global

Comparison

Evaluation

Validation

ABSTRACT

The Visible Infrared Imaging Radiometer Suite (VIIRS) Global Land Surface Phenology (GLSP) product (VNP22Q2 C2) has been operationally produced since 2013, and is designed to provide annual measurements of the phenologies of vegetated land surfaces at the global scale, succeeding the Moderate Resolution Imaging Spectroradiometer (MODIS) Land Cover Dynamics (LCD) product (MCD12Q2 C61), which was first produced in 2001. Although separate validations have been conducted locally to ensure the reliability and accuracy of the detected phenometrics for each product, a comprehensive understanding of the differences between these two operational products is important for downstream applications. Therefore, this study conducted critical analyses and cross-comparisons of the land surface phenology (LSP) products to ensure long-term continuity in the global phenological dynamics. Specifically, we compared five LSP products at 500 m spatial resolution: two NASA operational products of MCD12Q2 C61 and VNP22Q2 C2, as well as three other LSP products that were generated by applying the VNP22Q2 C2 algorithm to different time series from NOAA-20 VIIRS only, both SNPP and NOAA-20 VIIRS, and MODIS on Aqua and Terra. First, we cross-validated the five products at 500 m using a high-quality reference LSP dataset at 30 m that was generated by fusing the Harmonized Landsat and Sentinel-2 (HLS) observations with near-surface PhenoCam time series across diverse ecosystems in North America, Europe, and Japan. Second, cross-comparisons were conducted between the five LSP products at 500 m across 12 golden tiles. Third, the long-term comparability and continuity between the MCD12Q2 C61 and the VNP22Q2 C2 products were assessed globally. These comprehensive evaluations demonstrated that the VNP22Q2 C2 product provides overall global continuity for the MCD12Q2 C61 record. Compared to independent reference data from the HLS-PhenoCam LSP product, the four LSP products derived from the VNP22Q2 C2 algorithm produced highly comparable results with a mean absolute difference (MAD) of ~ 11 days and mean systematic bias (MSB) of ~ 7 days. The cross-comparisons indicated a strong agreement among the five 500 m LSP products in the 12 selected golden tiles with MADs < 7 days; however, their agreement with the MCD12Q2 C61 was slightly lower with MADs ~ 9–10 days. The global-scale evidence of continuity between the MCD12Q2 C61 and VNP22Q2 C2 products was an absolute difference of < 15 days, except in arid/semiarid, tropical, and high-latitude ecosystems. Finally, it is suggested that (1) the continuity from MODIS to VIIRS LSP products would be enhanced if the same phenological detection algorithm was applied to the MODIS data, and (2) the quality of the VIIRS GLSP product could be improved by integrating data from multiple VIIRS sensors.

* Corresponding authors at: Geospatial Sciences Center of Excellence, Department of Geography and Geospatial Sciences, South Dakota State University, Brookings, SD 57007, USA.

E-mail addresses: khuong.tran@nasa.gov (K.H. Tran), xiaoyang.zhang@sdstate.edu (X. Zhang).

1. Introduction

Vegetation phenology reflects a sequence of recurrent biological events in plant growth, such as budburst, leaf-out, growth, senescence, and leaf-fall (Richardson et al., 2013). In contrast to a few limited ground observations for specific plant species, land surface phenology (LSP) has been increasingly retrieved from satellite observations across broad spatial scales over the past four decades (Justice et al., 1985; Zhang et al., 2003; Henebry and de Beurs, 2025). LSP has been widely recognized as a key indicator of ecosystem and climate dynamics (Cleland et al., 2012; Chen et al., 2022; Morisette et al., 2009). It provides long-term and consistent measurements of large-scale phenological dynamics, which are fundamental for understanding the exchanges of carbon, water, and energy fluxes in global ecosystems and the regulation of terrestrial feedback between the land and atmosphere (Adole et al., 2016; Berra and Gaulton, 2021; Stucky et al., 2018).

The Advanced Very High Resolution Radiometer (AVHRR) onboard the series of NOAA (National Oceanic and Atmospheric Administration) satellites has delivered the longest-running LSP product, observing the global vegetation growing season's start and end using over 30 years of measurements from 1982 to 2013 (Julien and Sobrino, 2009; White et al., 2009; Wu et al., 2021). However, the coarse spatial resolution (≥ 1.1 km), inadequate radiometric calibration, inaccurate masks of snow and cloud cover, wide spectral bands, and positional inaccuracies cause significant uncertainty in the vegetation index derivations and phenological detections (Gutman, 1999; Nagol et al., 2009; de Beurs and Henebry, 2008; Sulla-Menashe et al., 2018). Notably, the Moderate Resolution Imaging Spectroradiometer (MODIS) onboard National Aeronautics and Space Administration (NASA)'s Terra (since 1999) and Aqua (since 2002) platforms has offered daily observations at 250–1000 m since 2000 (Ganguly et al., 2010). Particularly, the global MODIS Land Cover Dynamics (LCD) product (MCD12Q2) has been operationally produced annually at 500 m pixels since 2001 (Friedl et al., 2014; Gray et al., 2019). As both MODIS sensors have far surpassed their original five-year design lifespan and are planned for decommissioning, NASA has continuously produced a Global Land Surface Phenology (GLSP) product at 500 m since 2013 using the Visible Infrared Imaging Radiometer Suite (VIIRS) sensors onboard the Suomi National Polar-orbiting Partnership (SNPP) satellite (launched in October 2011) (Zhang et al., 2020b; Zhang et al., 2018). The VIIRS GLSP product (VNP22Q2) is proposed to ensure continuous measurement with the MODIS LCD (MCD12Q2) product, providing a sustained, scientifically reliable data record for various applications, such as global modeling and forecasting, ecological and environmental monitoring, and climate change research (Justice et al., 2013; Moon et al., 2019; Zhang et al., 2018).

The MODIS LCD and VIIRS GLSP products provide eleven similar phenological metrics (phenometrics) that are extracted from the two-band Enhanced Vegetation Index (EVI2) time series. These phenometrics are six phenological transition dates—greenup onset (the date when the plant starts to emerge new leaves and begins active photosynthesis), maturity onset (the date when the plant reaches to maximum green vegetation cover and photosynthetic activity), senescence onset (the date when the plant starts to lose leaves and photosynthetic activity begins to decrease sharply), dormancy onset (the date when the plant enters a state of physiological rest with minimal activity), and dates at mid greenup phase and mid senescence phase—and five greenness metrics—the EVI2 at the onset when vegetation starts to green up, the EVI2 at the onset when vegetation reaches greenness peak, the accumulated EVI2 value throughout the growing season, the rate of greenness accelerates, and the rate of greenness decelerates (Gray et al., 2019; Zhang et al., 2020b). However, differences in the detected phenometrics between these two products are unavoidable because they are generated from distinct instruments and they also use different phenological detection algorithms. Specifically, the MODIS LCD product applies (1) weighted cubic smoothing splines to fit the EVI2 data calculated from

MODIS nadir BRDF (bidirectional reflectance distribution function (BRDF)-Adjusted reflectance (NBAR) product, and (2) detects phenological timings using a set of thresholds on the fitted EVI2 time series (Gray et al., 2019). Whereas the VIIRS GLSP product uses (1) the Hybrid Piecewise Logistic Model (HPLM) to smooth the VIIRS NBAR EVI2 time series, and (2) the rate of change in curvature from the fitted EVI2 time series to identify phenological timings (Zhang et al., 2018).

Systematic evaluations examining the consistency between the MODIS LCD and VIIRS GLSP products are generally lacking (but see de Beurs et al., 2025). Previous validation efforts focused on the reliability and accuracy of the detected phenometrics on each product separately using independent ground-based observations of related phenomena, such as the eddy flux tower measurements of Gross Primary Production, the PhenoCam Network, and the national/continental phenology networks (Klosterman et al., 2014; Ganguly et al., 2010; Ye et al., 2022; Shen et al., 2021), and other satellite-based LSP products at higher spatial resolutions, such as Landsat and Harmonized Landsat and Sentinel (HLS) phenometrics at 30 m pixels (Moon et al., 2019; Bolton et al., 2020; Zhang et al., 2018; Zhang et al., 2017). However, it remains challenging to use either ground-based observations or finer-scale LSP products to validate the accuracy of the MODIS LCD and VIIRS GLSP products due to four key reasons. First, the MODIS/VIIRS phenology products estimate the phenological dynamics of the vegetated land surface within a large spatial footprint (i.e., 500 m), which generally contains a variety of plant species and characteristics, diverse growing environments, and local climates (Tran et al., 2022). Second, available phenological networks (i.e., the United States National Phenology Network – US NPN) only provide ground measurements for a few specific plants in regional areas that are difficult to aggregate to MODIS/VIIRS pixel-based phenologies for direct comparison (Vrieling et al., 2017; Ye et al., 2022). Third, although cooperative continental-scale phenological observatory (e.g., the PhenoCam network) offer accurate top-canopy phenologies in various ecosystems, the mismatch in viewing geometry and area coverage complicates direct comparisons with satellite-based observations, especially in heterogeneous landscapes, mixtures of plant species, and sharp gradients of terrain and climates, particularly in mountains (Li et al., 2017; Melaas et al., 2018). Fourth, incomplete satellite time series with large temporal gaps have been identified as a primary source of uncertainty in phenology detections (Tran et al., 2022; Zhang et al., 2009). Higher spatial resolution data (e.g., Landsat/Sentinel-2) generally have longer revisit times than MODIS/VIIRS, which makes it unsuitable to quantify the accuracy of MODIS/VIIRS phenometrics using these data (Shen et al., 2021; Zhang et al., 2020a).

Moon et al. (2019) performed an initial product-to-product comparison to evaluate the systematic discrepancies between two global phenological products in North America (the MODIS LCD and VIIRS GLSP), coupled with evaluations using independent data from Landsat and PhenoCam. Their results showed that the MODIS LCD product agrees well with the VIIRS GLSP product. However, because (1) prior analyses were based on only three tiles, and (2) both Landsat with longer revisit times and PhenoCam imagery with spatial mismatches could introduce systematic biases and uncertainties in results from these analyses, it is premature to conclude that the VIIRS GLSP product provides a strong foundation for continuity that extends the long-term LSP times series provided by the MODIS LCD products. Specifically, inconsistencies between the MODIS LCD and VIIRS GLSP products could generate discrepancies in the phenometrics, leading to uncertainties in downstream applications. Thus, there is a pressing need to rigorously evaluate both quantitatively and qualitatively the precision, accuracy, consistency, and continuity in the LSP products that are generated from the MODIS and VIIRS sensors. Furthermore, NOAA launched VIIRS sensors aboard the NOAA-20 satellite in November 2017 and the NOAA-21 satellite in November 2022 into early afternoon orbits to ensure the continuous operation of satellite observations and products (Lyapustin et al., 2023). Currently, the VIIRS GLSP product (VNP22Q2) has been

processed from VIIRS SNPP only, while the MODIS LCD (MCD12Q2) product has been processed using the MODIS onboard Aqua (1330 nominal overpass) and Terra (1030 nominal overpass) (Román et al., 2024).

It is also crucial to ensure the continuity of GLSP products derived from the VIIRS aboard SNPP, NOAA-20, and NOAA-21, since these satellites play a vital role in maintaining the consistency of long-term environmental monitoring and phenological measurements. Given that temporal gaps, which are associated with persistent snow, cloud cover, and other factors, can significantly degrade the precision of phenological detections, it is essential to explore whether combining data from different VIIRS sensors could provide a single high-quality VIIRS time series for consistently retrieving LSP. Therefore, in this study, we evaluated the 500 m VIIRS GLSP products using a high-quality reference of LSP dataset at 30 m pixels produced from a fusion of HLS data and near-surface PhenoCam time series (Tran et al., 2023a). We then conducted cross-comparisons between the 500 m MODIS/VIIRS phenology products across 12 golden tiles that were selected for intensive analysis and validation of global remote sensing products (Román et al., 2024). Third, we assembled and evaluated evidence at a global scale regarding the long-term continuity between the operational MCD12Q2 C61 and the VNP22Q2 C2 products.

2. Data and methods

2.1. Study area

This study evaluated the continuity of the 500 m MODIS/VIIRS phenology products across the globe (Fig. 1). Specifically, we performed three unique analyses. First, the quality of the 500 m LSP products was initially assessed based on 15 MODIS tiles where the 30 m HLS-PhenoCam LSP product was available in 89 sites (10 km × 10 km coverage at each site) (Section 2.2.2). This assessment included 12 tiles covering 78 HLS-PhenoCam sites in North America, two tiles covering

seven sites in Europe, and one tile covering four sites in Japan. Second, cross-comparisons between the five 500 m LSP products were organized over the 12 golden tiles consisting of h09v05, h11v03, and h13v02 in North America; h11v08 and h11v11 in South America; h17v07 and h20v11 in Africa; h19v02 and h21v02 in Europe; h24v04 and h26v04 in Asia; and h30v11 in Australia (Román et al., 2024, yellow squares in Fig. 1). Third, the continuity between two NASA operational products (MCD12Q2 C61 and VNP22Q2 C2) was performed across the global land surface.

2.2. Datasets

2.2.1. The 500 m LSP products

This study primarily analyzed five 500 m MODIS/VIIRS phenology products. Four of them were generated by applying the VNP22Q2 C2 algorithm to different inputs from the MODIS/VIIRS time series (Fig. 2). Specifically, the VNP22Q2 C2 algorithm has been used to produce the VIIRS GLSP product (VNP22Q2 C2) from the daily VIIRS SNPP NBAR product on an operational basis since 2013. Following a three-step process, the VNP22Q2 C2 algorithm was developed based on the HPLM-LSPD (Land Surface Phenology Detection) algorithm (Zhang, 2015). Briefly, the VNP22Q2 C2 algorithm first processes the raw VIIRS SNPP NBAR product (VNP43I) to obtain the time series of 3-day composite EVI2. Although the VIIRS provides observations daily, the derived 3-day EVI2 time series regularly contains temporal gaps due to persistent cloud or snow cover, atmospheric contamination, and instrument-related factors (Zhang et al., 2020a). To reduce these gaps, the Spatio-temporal Shape-Matching Model (SSMM) (Zhang et al., 2021) is integrated to fuse the derived SNPP EVI2 time series with the most comparable shape of the EVI2 climatology, which is “gap-free average” EVI2 calculated from the MODIS NBAR data from 2013 to 2019. Second, the algorithm calculates background EVI2 values that represent the maximum EVI2 value during the period after snowmelt but before vegetation growth (Zhang, 2015), and it smooths the EVI2 time series

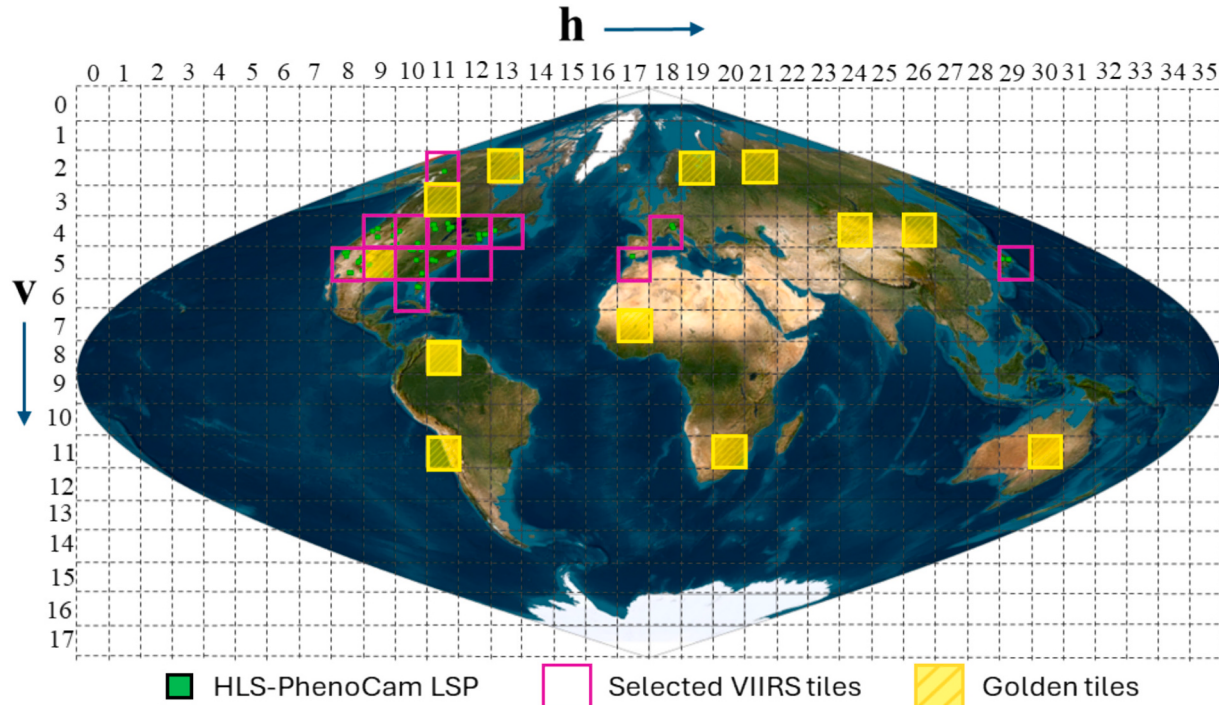


Fig. 1. Cross-comparisons between the MODIS Land Cover Dynamics (MCD12Q2 C61) product and the VIIRS Land Surface Phenology (VNP22Q2 C2) product are conducted globally. The map shows 12 golden tiles, and 89 sites of the HLS-PhenoCam LSP across North America, Europe, and Japan that are overlapped by 15 VIIRS tiles for the comparison. The green rectangles indicate HLS-PhenoCam LSP sites, which are enlarged for visibility. (For interpretation of the references to colour in this figure legend, the reader is referred to the web version of this article.)

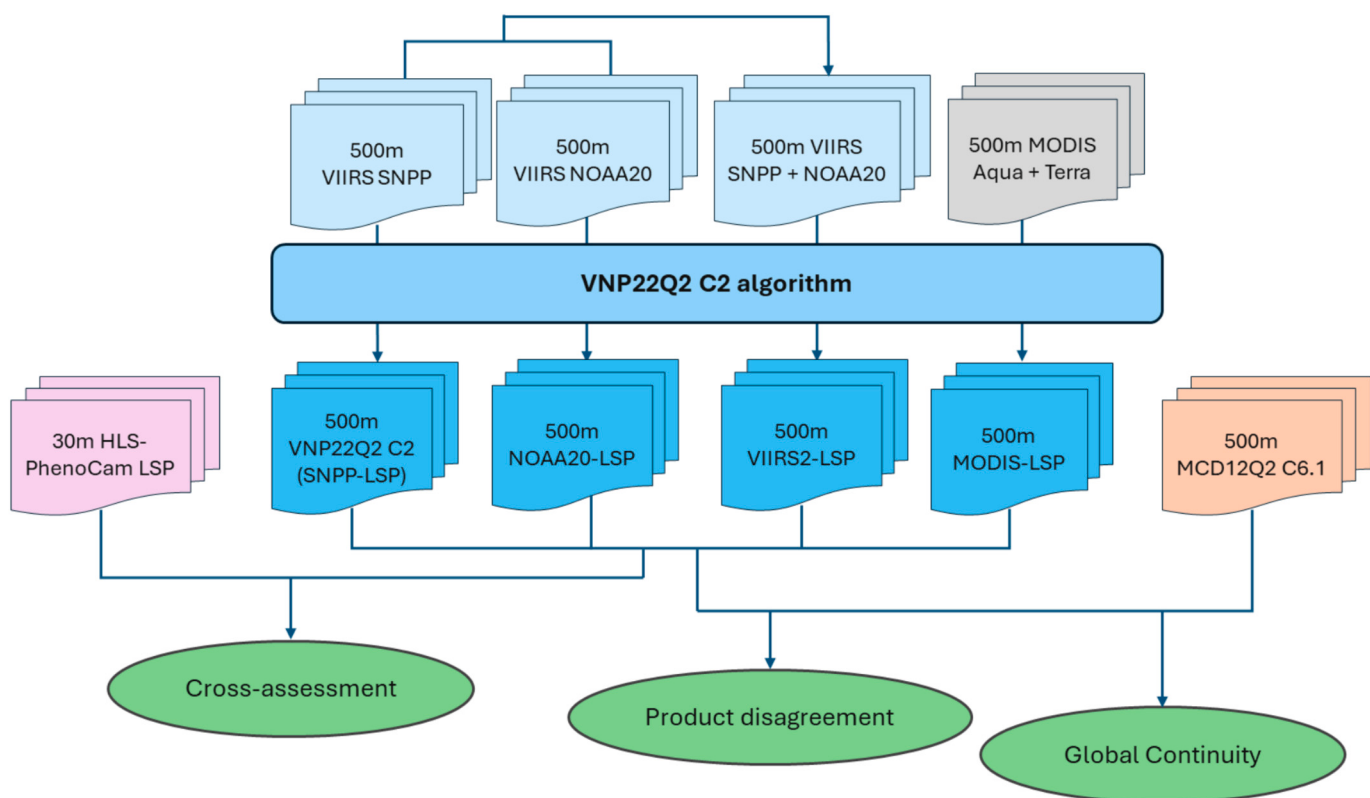


Fig. 2. Workflow to assess the accuracy and global continuity and consistency of the phenological products derived from MODIS and VIIRS sensors.

using three filters: Savitzky-Golay, moving average, and moving median. Third, the VNP22Q2 C2 algorithm uses the HPLM to fit the smoothed time series in greenup and senescence phases. Two pairs of minimum and maximum extremes in the greenup and senescence phases are identified using the rate of change in curvature calculated from the HPLM fitted EVI2 time series, which correspond to the four key phenological timings: onsets of greenup, maturity, senescence, and dormancy (Zhang et al., 2003; Zhang et al., 2006). Other phenometrics, such as the maximum and minimum EVI2 values, rate of change in EVI2 values, and growing season lengths are extracted and included in the VNP22Q2 C2 product (<https://lpdaac.usgs.gov/products/vnp22q2v002/>). Since the operational VNP22Q2 C2 product is generated primarily from the VIIRS SNPP time series, it is hereafter referred to as the SNPP-LSP product to distinguish it from other 500 m LSP products based on different sensors.

We also applied the VNP22Q2 C2 algorithm to generate three other products using different EVI2 inputs: (1) NOAA20-LSP from VIIRS NOAA-20 NBAR product (VJ143IA4); (2) VIIRS2-LSP from the combination of VIIRS SNPP NBAR and NOAA-20 NBAR products; and (3) MODIS-LSP from the Terra and Aqua MODIS NBAR products (MCD43A4). Comparison of these products allowed us to ensure if the GLSP products generated using the same VNP22Q2 C2 algorithm from different sensors exhibit superior continuity. Note that NOAA-21 was not involved in our analyses, as it only began collecting data in early 2023.

The MCD12Q2 C61 product, in contrast, is generated by a different algorithm (Gray et al., 2019). This algorithm initially calculates the background EVI2 values from the MODIS NBAR (MCD43A4) to mitigate the effects of snow-contaminated observations and possible land cover changes during the dormant period. Second, a penalized cubic smoothing spline fits the EVI2 time series proportionally weighted to the quality assurance (QA/QC) flags from the MCD43A2 product. Third, relative EVI2 thresholds are applied to detect key phenological timings, which are greenup and maturity onsets when the EVI2 at 15 % and 90 %

of the EVI2 amplitude in greenup phase and senescence and dormancy onsets at 90 % and 15 % of the EVI2 amplitude in the greendown phase. Other greenness phenometrics, similar to the VNP22Q2 product, are included in the MCD12Q2 C61 product. The product has been generated at 500 m (<https://lpdaac.usgs.gov/products/mcd12q1v061/>).

2.2.2. The 30 m HLS-PhenoCam LSP product

The HLS-PhenoCam LSP product at 30 m was used as a high-quality reference dataset to cross-validate the 500 m LSP products. The HLS-PhenoCam LSP product has been recently produced by fusing HLS data with PhenoCam time series (Tran et al., 2023a, 2022). Briefly, although the HLS provides observations at 2–3 day intervals, their EVI2 time series often experiences temporal gaps caused by persistent cloud or snow cover, instrument-related artifacts, and atmosphere effects (Shen et al., 2021). The PhenoCam network captures half-hourly top-of-canopy RGB (Red, Green, and Blue) images without degradation due to cloud cover, and enables extraction of a Green Chromatic Coordinate (GCC = G/(R + G + B)) time series for tracking apparent canopy phenology at over 700 sites globally (Brown et al., 2016; Richardson, 2023). Because diverse phenological behaviors commonly exist within local areas, the PhenoCam image in each site is divided into 100 equal grids to extract a collection containing many grid-based gap-free GCC time series with various temporal shapes. For a given HLS pixel, the SSMM searches the most comparable GCC temporal shape in the derived collection to pair and fuse with the considering HLS EVI2 time series. This approach is able to generate the blended HLS-PhenoCam EVI2 time series at 30 m pixels with no gaps across the region. The four key phenological onsets of greenup, maturity, senescence, and dormancy are then extracted from the fused HLS-PhenoCam EVI2 time series using the HPLM-LSPD. The HLS-PhenoCam LSP product currently covers 78 regions (each spanning an area of 10 km by 10 km) across diverse ecosystems in the United States (US) with an accuracy of < 5 days during 2019 and 2020, which is publicly distributed via the NASA Oak Ridge National Laboratory Distributed Active Archive Center (ORNL DAAC)

(doi:<https://doi.org/10.3334/ORNLDAA/2248>; Tran et al., 2023b). Furthermore, we applied the framework developed by Tran et al. (2022) to extend the HLS-PhenoCam LSP product by fusing the HLS observations with the PhenoCam data in Europe (7 regions) and with the near-surface Phenological Eyes Network data (PEN, <http://www.pheno-eye.org/>) in Japan (4 regions) (Fig. 1).

2.2.3. The MODIS land cover type

The MODIS Land Cover Type (MCD12Q1) version 6.1 product was used as an ancillary dataset (<https://lpdaac.usgs.gov/products/mcd12q1v061/>). Specifically, the MCD12Q1 uses a decision tree classifier for the supervised classification of MODIS Terra and Aqua NBAR data to generate global land cover maps annually from 2001 to 2022. The accuracy of specific classes is enhanced by post-processing processes using the prior knowledge and ancillary data (Friedl et al., 2010, 2002). The MCD12Q1 product has been intensively used in various studies and applications (de Almeida et al., 2016; Mu et al., 2011; Pérez-Hoyos et al., 2017; Wan, 2008; Yan et al., 2016; Zhang and Roy, 2017). Of the five classification schemes available in MCD12Q1, the International Geosphere-Biosphere Programme (IGBP) option was used here. The IGBP scheme provides 17 land cover types (LCTs): three developed and mosaicked land classes, three non-vegetated land classes, and 11 natural vegetation classes (Loveland and Belward, 1997).

2.3. Analysis workflow

This study conducted three analyses to assess the long-term global continuity of the phenological dynamics derived from the MODIS and VIIRS sensors (Fig. 2). We first used the 30 m HLS-PhenoCam LSP product for the years 2019 and 2020 as an independent and high-quality reference to cross-validate the four 500 m LSP products derived from the VNP22Q2 C2 algorithm. Subsequently, we evaluated the disagreement among these five 500 m LSP products for three years from 2019 to 2021 through cross-comparisons of the phenometrics derived from different phenological detection algorithms and MODIS/VIIRS time series inputs. Finally, we examined the discrepancy and continuity between the NASA operational LSP products—MODIS LCD and VIIRS GLSP—globally for 2019 and 2020.

2.3.1. Cross-validation of the 500 m LSP products using 30 m HLS-PhenoCam LSP product

The HLS-PhenoCam LSP product at 30 m spatial resolution was selected to cross-validate the four LSP products at 500 m pixels derived from the VNP22Q2 C2 algorithm. Due to differences in the projection and spatial extent between the 500 m MODIS/VIIRS LSP products (the actual pixel size is 463.5 m) and the 30 m HLS-PhenoCam LSP product, we first reprojected these 500 m LSP products from its native sinusoidal projection to the UTM with a spatial resolution of 450 m that corresponds to 15 HLS pixels, and then clipped the reprojected products to generate 89 subsets of 10 km × 10 km that were co-located with the HLS-PhenoCam LSP products. The reprojection of 500 m products was to resample the size that could match well with the aggregation of 30 m pixels, which was chosen in previous studies showing promising results (Zhang et al., 2020a; Bolton et al., 2020; Moon et al., 2019). Specifically, the subsets included 78 in North America distributed over 13 MODIS/VIIRS tiles, seven in Europe over two tiles, and four in Japan over one tile (Fig. 1). To reduce geolocation errors among sensors and projection differences, the preprocessed MODIS/VIIRS phenology products at 450 m were compared with the HLS-PhenoCam LSP product averaged using a 3 × 3450 m moving window (Zhang et al., 2020a; Bolton et al., 2020). A mutual mask was then applied to remove all non-valid samples for a comparable evaluation of the 500 m LSP products. Thus, the averaged HLS-PhenoCam phenometrics were used to assess the SNPP-LSP, NOAA20-LSP, VIIRS2-LSP, and MODIS-LSP for the years 2019 and 2020 using scatterplots and metrics of disagreement. Note that the MCD12Q2 C61 was not evaluated using the HLS-PhenoCam

phenometrics to avoid potential bias because they were generated from different algorithms. The Pearson correlation coefficient (r) [1], the mean absolute difference (MAD) [2], the root mean square difference (RMSD) [3], and the mean systematic bias (MSB) [4] were calculated across all samples derived from each of 89 subsets of 10 km × 10 km. The MAD and MSB were calculated separately for four key phenological transition dates.

$$r = \frac{\sum_{i=1}^N (X_i - \bar{X})(Y_i - \bar{Y})}{\sqrt{\sum_{i=1}^N (X_i - \bar{X})^2(Y_i - \bar{Y})^2}} \quad (1)$$

$$MAD = \frac{\sum_{i=1}^N |Y_i - X_i|}{N} \quad (2)$$

$$RMSD = \sqrt{\frac{\sum_{i=1}^N (Y_i - X_i)^2}{N}} \quad (3)$$

$$MSB = \frac{\sum_{i=1}^N (Y_i - X_i)}{N} \quad (4)$$

where X_i are the HLS-PhenoCam phenometrics and Y_i are phenometrics detected from either the 500 m LSP products, respectively, with their average values \bar{X} and \bar{Y} . N is the number of samples used in the calculation.

2.3.2. Cross-comparisons between the 500 m LSP products in the 12 golden tiles

Cross-comparisons estimated the consistency between the five 500 m LSP products. Similar to the cross-product assessment in Section 2.3.1, we applied a 3 × 3 moving average window of 500 m pixels that removed all non-valid samples from a mutual mask to reduce the geolocation error due to sensor differences. Specifically, the r, MAD, RMSD, and MSB (Eqs. [1]–[4]) were first calculated for each pair of 500 m LSP products for three years (2019–2021), leading to ten cross-comparisons among the five products in each golden tile.

Further, the average number of pixels with valid phenological detections between the VNP22Q2 C2 algorithm and MCD12Q2 C61 algorithm from 2019 to 2021 was compared in each golden tile. This step investigated differences in LSP detectability. Finally, LSP discrepancies among different sensors were examined by comparing the assessment results with the seasonal magnitudes of vegetation greenness. Specifically, the phenometric discrepancies between the SNPP-LSP and NOAA20-LSP products were analyzed against the variation in EVI2 greenness magnitude across each of the 12 golden tiles. The EVI2 greenness magnitude was the difference of EVI2 values between maturity onset and greenup onset, which was assumed to be comparable for MODIS/VIIRS sensors.

2.3.3. Comparison between the MCD12Q2 and the VNP22Q2 products at a global scale

To reveal the continuity between the NASA operational MCD12Q2 and the VNP22Q2 products across the globe, the difference was calculated between the VNP22Q2 C2 and MCD12Q2 C61, between the MODIS-LSP and MCD12Q2 C61, and between the VNP22Q2 C2 and MODIS-LSP for two years: 2019 and 2020. Pixel-based absolute differences were calculated for onsets of greenup, maturity, senescence, and dormancy. The resultant spatial patterns of absolute differences identified those regions with strong agreement, suggesting phenological continuity, as well as areas of significant discrepancy among the 500 m LSP products. Furthermore, the MADs of each phenological transition date between these 500 m LSP products were analyzed for each LCT. The analysis was applied to 15 of 17 LCTs with only open water and permanent snow/ice excluded. This stratified analysis enabled a more nuanced understanding of how LSP product agreement varies by biome.

3. Results

3.1. Assessment of the 500 m global LSP products derived from the VNP22Q2 C2 algorithm

Fig. 3 and **Table 1** present results comparing the four LSP products at 500 m (SNPP-LSP, NOAA20-LSP, VIIRS2-LSP, and MODIS-LSP) that were derived from the VNP22Q2 C2 algorithm, against independent high-quality HLS-PhenoCam phenometrics over 15 selected tiles across North America, Europe, and Japan (**Fig. 1**). The scatter plots indicated that phenological transition dates were consistently detected in all four LSP products with r values = 0.98, MADs \sim 11 days, RMSDs \sim 16 days, and MSBs \sim 7 days. The MAD and MSB values showed their accuracy was much higher in greenup, maturity, and dormancy onsets than in senescence onset (**Table 1**). The MADs were \sim 8 days for greenup onset, \sim 7 days for maturity onset, and \sim 9 days for dormancy onset; and the MSBs were \sim 5 days, \sim 2 days, and \sim 5 days. However, the senescence onset from all four LSP products was consistently earlier than that from the reference with MADs of 21–22 days and MSBs of 21–22 days.

Fig. 4 displays the spatial patterns of the MADs between the 500 m VIIRS2-LSP and the 30 m HLS-PhenoCam LSP reference in 2019 for each phenological metric across the 89 subsets. The pattern was similar for the other four 500 m LSP products because all the products had comparable differences with HLS-PhenoCam phenometrics. In the US, the MADs for greenup onset and maturity onset (**Fig. 4a** and b) were $<$ 15 days in northeastern and midwestern regions and $<$ 20 days in the southwestern and southeastern regions. Only a few locations showed MADs $>$ 25 days, mostly in drylands in the southwestern US and tropical humid areas (e.g., Florida). The MADs for senescence onset (**Fig. 4c**) were comparatively small ($<$ 20 days) in the central US, while they were

Table 1

The mean absolute differences (MADs) and mean systematic biases (MSBs) for each phenological onset derived from the cross-evaluation of detected LSP dates between the 500 m LSP products and the 30 m HLS-PhenoCam LSP product across 15 selected VIIRS tiles in North America, Europe, and Japan (**Fig. 1**) for 2019 and 2020. Units for MAD and MSB are days.

Phenometric	Metric	SNPP	NOAA20	VIIRS2	MODIS
Greenup onset	MAD	8.9	8.8	8.2	8.6
	MSB	-5.4	-5.5	-4.2	-4.7
Maturity onset	MAD	7.5	7.3	7.4	7.6
	MSB	3.0	2.2	2.8	2.6
Senescence onset	MAD	21.3	21.6	22.2	21.6
	MSB	-20.9	-21.3	-22.0	-21.4
Dormancy onset	MAD	9.3	9.5	9.5	9.2
	MSB	-4.8	-4.4	-5.4	-4.2

large ($>$ 25 days) in the western and eastern US. The MADs for dormancy onset (**Fig. 4d**) were mostly $<$ 20 days across northeastern and midwestern regions, while they were large ($>$ 20 days) in southwestern and tropical humid areas (e.g., Florida). In Europe, the MADs for greenup onset and maturity onset (**Fig. 4e** and f) were smaller than those for senescence and dormancy onsets (**Fig. 4g** and h). They were large for senescence and dormancy onsets ($>$ 30 days) in semiarid areas of Spain (**Fig. 4g** and h). In Japan, the MADs for all four phenological onsets (**Figs. 4i-l**) exhibited $<$ 20 days, except for senescence in one site showing a MAD $>$ 25 days (**Fig. 4k**).

3.2. Disagreement among the 500 m LSP products

Table 2 shows the average disagreement among the five LSP products

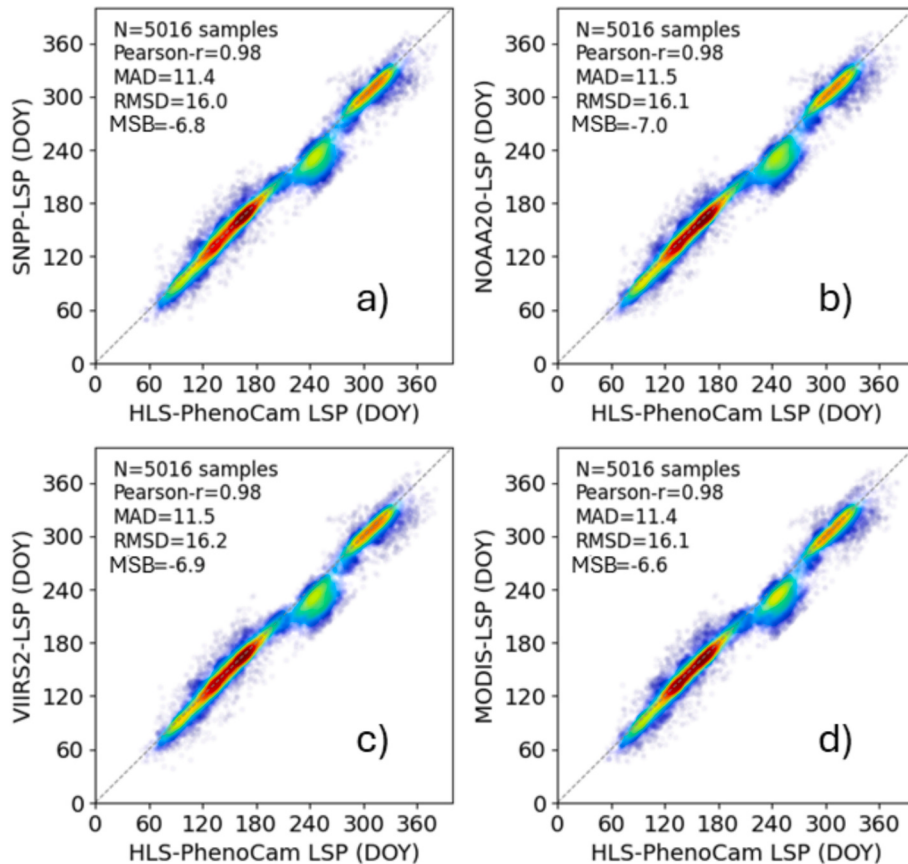


Fig. 3. A cross-validation of detected LSP dates between the four 500 m LSP products derived from the VNP22Q2 C2 algorithm and the independent 30 m HLS-PhenoCam LSP product across 15 selected VIIRS tiles in North America, Europe, and Japan (**Fig. 1**) for the years 2019 and 2020. The LSP products are the SNPP-LSP, NOAA20-LSP, VIIRS2-LSP, and MODIS-LSP, respectively. Each sample corresponds to a 3×3450 m-pixel window for four phenological transition dates.

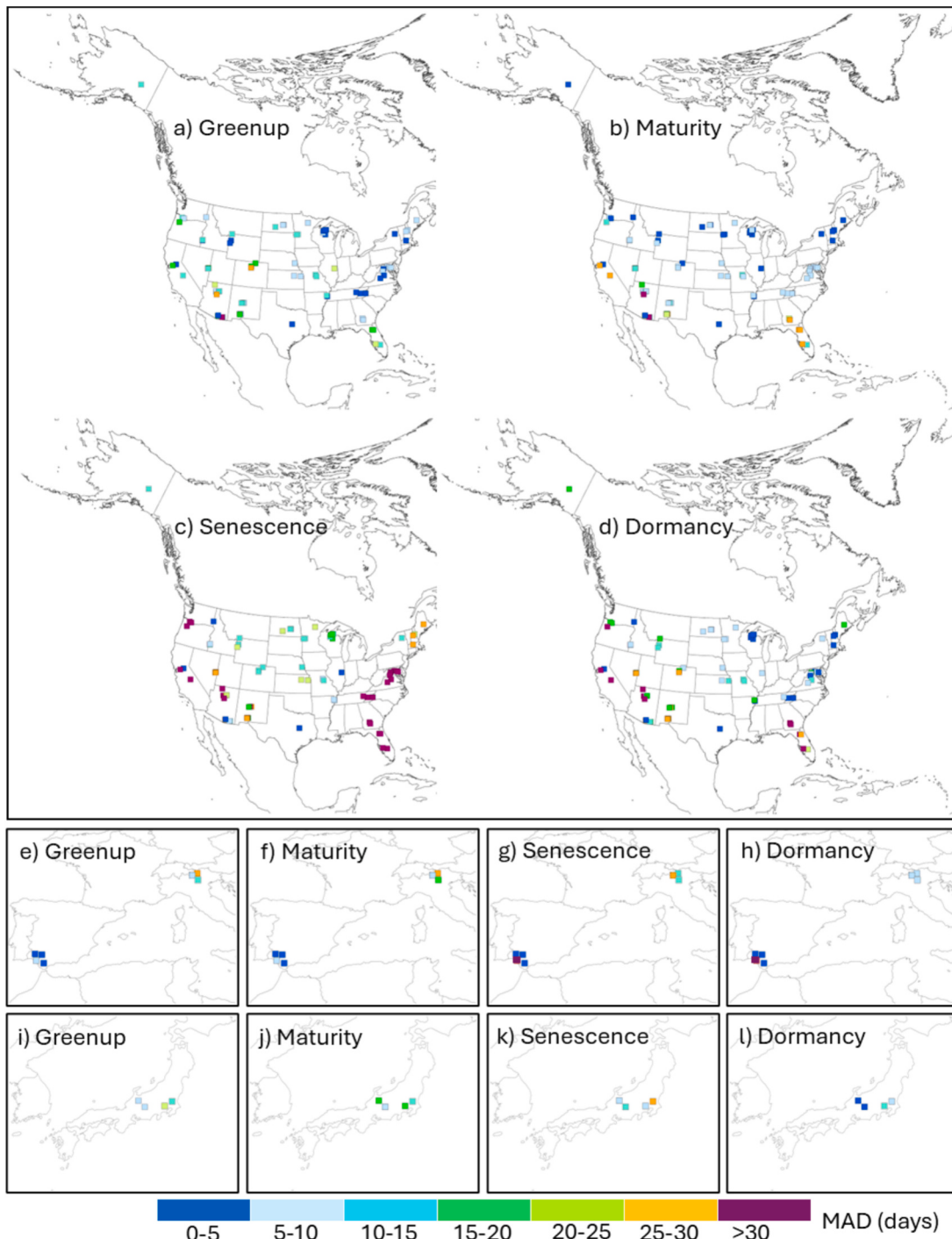


Fig. 4. Spatial patterns of the mean absolute differences (MADs) between the 500 m VIIRS2-LSP and the 30 m HLS-PhenoCam LSP in 2019 for each phenological onset across the HLS-PhenoCam sites ($10 \text{ km} \times 10 \text{ km}$) in North America (a-d), Europe (e-h), and Japan (i-l). The rectangles represent HLS-PhenoCam LSP sites, which are enlarged for visualization purposes.

over the 12 golden tiles. Overall, the four LSP products derived from the VNP22Q2 C2 algorithm achieved very low disagreement, with $\text{MADs} < 7 \text{ days}$, $\text{RMSDs} < 10 \text{ days}$, and $\text{MSBs} < 1 \text{ day}$. While they showed marginally higher disagreement with the MCD12Q2 C61, with $\text{MADs} \sim 9\text{--}10 \text{ days}$, $\text{RMSDs} \sim 10\text{--}15 \text{ days}$, and $\text{MSBs} < 1 \text{ day}$. The spatial patterns of their disagreements appear in Table S1, displaying the cross-comparisons among the five LSP products in the 12 golden tiles from 2019 to 2021. Specifically, the disagreements were lower in 6 out of 12 tiles (h11v03, h11v11, h17v07, h20v11, h24v04, and h26v04) with $\text{MADs} < 10 \text{ days}$, $\text{RMSDs} < 14 \text{ days}$, and $\text{MSBs} < 3 \text{ days}$. Relatively

larger discrepancies occurred in Australia (h30v11) with MAD as large as 13 days, RMSD as large as 19 days, and MSB as large as 8 days; western US (h09v05) with MAD as large as 10 days, RMSD as large as 15 days, and MSB as large as 2 days; and in tropical forests (h11v08) with MAD as large as 15 days, RMSD as large as 21 days, and MSB as large as 5 days. Furthermore, three tiles (h13v02, h19v02, and h21v02) in high-latitude areas showed four products derived from the VNP22Q2 C2 algorithm obtained very low disagreement with $\text{MADs} < 6 \text{ days}$, $\text{RMSDs} < 8 \text{ days}$, and $\text{MSBs} < 2 \text{ days}$. However, their disagreement with the MCD12Q2 C61 product was lower with $\text{MADs} < 20 \text{ days}$, $\text{RMSDs} < 30$

Table 2

Average metrics of disagreement of detected LSP dates among the five 500 m LSP products in the 12 golden tiles from 2019 to 2021.

		NOAA20-LSP	VIIRS2-LSP	MODIS-LSP	MCD12Q2
SNPP-LSP	r	0.99	0.99	0.99	0.98
	MAD	6.8	4.7	6.5	10.3
	RMSD	9.8	6.9	9.1	14.9
	MSB	-0.7	-0.2	-0.5	-0.9
NOAA20-LSP	r	0.99	0.99	0.99	0.98
	MAD	4.3	6.0	10.2	
	RMSD	6.2	8.3	14.8	
	MSB	0.1	-0.2	-0.5	
VIIRS2-LSP	r	0.99	0.99	0.98	
	MAD		6.0	10.2	
	RMSD		8.4	14.9	
	MSB		-0.8	-0.6	
MODIS-LSP	r		0.98		
	MAD		9.4		
	RMSD		14.1		
	MSB		-0.4		

days, and MSBs < 4 days.

Fig. 5 presents scatterplots of phenometrics detected from the operational VNP22Q2 C2 product and the MCD12Q2 C61 product over the 12 golden tiles for the years 2019 and 2020. Overall, the VNP22Q2 C2 product agreed well with the MCD12Q2 C61 product. Specifically, 6 out of 12 tiles (h11v03, h11v11, h17v07, h20v11, h24v04, and h26v04) showed MADs < 9 days, RMSDs < 12 days, and MSBs < 3 days. Relatively larger differences occurred in arid Australia (h30v11) with MADs ~ 13 days, RMSDs ~ 18 days, and MSB ~ 9 days; western US (h09v05) with MAD ~ 10 days, RMSD ~ 15 days, and MSB < 1 day; as well as in tropical forests (h11v08) with MAD ~ 15 days, RMSD ~ 21 days, and MSB ~ 3 days. The disagreement was higher for the three high-latitude tiles (h13v02, h19v02, and h21v02) with MADs > 13 days, RMSDs > 18 days, and MSBs < 2 days. This large difference was due to a much earlier greenup onset and much later dormancy detected at these high latitudes in the MCD12Q2 C61 product: the greenup onset was detected before DOY (day of year) 90, i.e., before April, and dormancy onset was detected after DOY 300, i.e., after October.

Fig. 6 displays the count of pixels that have valid phenological detections. The number was generally equivalent in the four products derived from the VNP22Q2 C2 algorithm in each golden tile, while the MCD12Q2 C61 product showed slightly fewer detections in tropical and mid to high latitudes (h11v08, h17v07, h11v03, h13v02, h19v02, and h21v02) and significantly fewer detections in arid and semiarid ecosystems (h09v05, h11v11, h30v11).

Fig. 7 displays the MADs between the SNPP-LSP and NOAA20-LSP as a function of EVI2 magnitudes across all golden tiles from 2019 to 2021. The MAD of all four phenological onsets decreased linearly with EVI2 magnitude. The MAD was < 15 days when the EVI2 magnitude was > 0.1; however, the phenological detections were less reliable (MADs > 22 days) when the EVI2 magnitude was < 0.05.

3.3. Continuity between the 500 m LSP products across the global land surface

To assess global phenological continuity and detect spatial inconsistencies among satellite-derived LSP products, we analyzed absolute differences in key transition dates between the MODIS and VIIRS phenological products. Fig. 8 shows the global patterns of the absolute differences in 2019: between the two operational VNP22Q2 C2 and the MCD12Q2 C61 products (left column), between the MODIS-LSP and the MCD12Q2 C61 products (middle column), and between VNP22Q2 C2 and the MODIS-LSP products (right column). Overall, despite regional discrepancies, strong agreements between the 500 m LSP products were evident, suggesting continuous and consistent phenological patterns in the transition from MODIS to VIIRS sensors across most global regions.

The stronger agreement occurred for maturity and senescence onsets, as these tended to be more comparable across products than greenup and dormancy onsets. Moreover, the analysis revealed three notable patterns that highlight key differences and similarities among the products across various regions and phenological stages. First, the VNP22Q2 C2 product was highly comparable with the MCD12Q2 C61 product globally. However, the maturity and senescence onsets had relatively large differences (> 15 days) in the tropical regions in Asia and Africa and arid and semiarid areas in South America (Fig. 8b and c), and the greenup and dormancy onsets exhibited large discrepancies in high-latitude regions (Fig. 8a and d). In addition, the VNP22Q2 C2 product showed more phenology detections than the MCD12Q2 C61 product in the western US, South America, Central Asia, and Australia (Fig. 8). Second, the spatial differences between the MODIS-LSP and MCD12Q2 C61 products were similar to those between the VNP22Q2 C2 and the MCD12Q2 C61 products (Figs. 8e-h). The smaller absolute differences were highlighted across the globe, which was < 7 days in many regions, such as North America, South America, Africa, Europe, Asia. However, the large differences remained in high-latitude, tropical, and arid and semiarid areas. Third, the absolute differences between VNP22Q2 C2 and the MODIS-LSP products were typically less than two weeks for most of the areas around the world (Figs. 8i-l), although relatively larger differences often occurred in some arid and semiarid areas in South America and tropical areas in Africa and Southeast Asia, highlighting the ongoing challenge of capturing phenology in ecologically and climatically complex regions.

Fig. 9 shows bar plots and statistics of the MADs from the four key phenological timings between the VNP22Q2 C2 and the MCD12Q2 C61 products, between the MODIS-LSP and MCD12Q2 C61 products, and between the VNP22Q2 C2 and MODIS-LSP products across the 15 LCTs for 2019 and 2020. The differences between the VNP22Q2 C2 and MCD12Q2 C61 products included: (1) the MADs were mostly < 20 days for every LCT except evergreen broadleaf forests; (2) the MADs were lowest in deciduous and mixed forests (< 12 days), followed by evergreen needleleaf forests, savannas, cropland, and barren/sparse vegetated groups with MADs of ~ 15 days; (3) the MADs were slightly higher (~ 18 days) in urban, shrubland, and wetland LCTs, which included typically higher MADs in greenup and dormancy onsets in shrublands than in maturity and senescence onsets; and (4) extremely large MADs of > 30 days occurred in evergreen broadleaf forests. Statistical results in Fig. 9c also indicated the VNP22Q2 C2 product was more comparable with the MODIS-LSP than with the MCD12Q2 C61 product across all LCTs. The discrepancies between the VNP22Q2 C2 product and the MODIS-LSP product were relatively small across all LCTs. The corresponding MADs were < 10 days in deciduous and mixed forests, open shrublands, barren/sparse vegetated groups, < 15 days in closed shrublands, woody savannas, savannas, grasslands, permanent wetlands, croplands, and evergreen needleleaf forest, ~ 17 days in urban areas and cropland/natural vegetation mosaics, and > 25 days in evergreen broadleaf forest.

4. Discussion

This multipart study provided complementary evaluations and critical need for the global continuity of the phenology products derived from the MODIS and VIIRS sensors, because the widely used MODIS Land Cover Dynamics (LCD) product (MCD12Q2) is expected to be decommissioned in the near future and the VIIRS LSP product will succeed in continuity. The significance and novelty in this study can be simply summarized as the following. First, it evaluated four LSP products (SNPP-LSP from SNPP only, NOAA20-LSP from NOAA-20 only, VIIRS2-LSP from both SNPP and NOAA-20, and MODIS-LSP from MODIS data) that were derived from the VNP22Q2 C2 algorithm and NASA MODIS LCD product (MCD12Q2 C61) for global 12 golden tiles and evaluated the products using the newly developed HLS-PhenoCam LSP dataset spanning North America, Europe, and Asia. The result

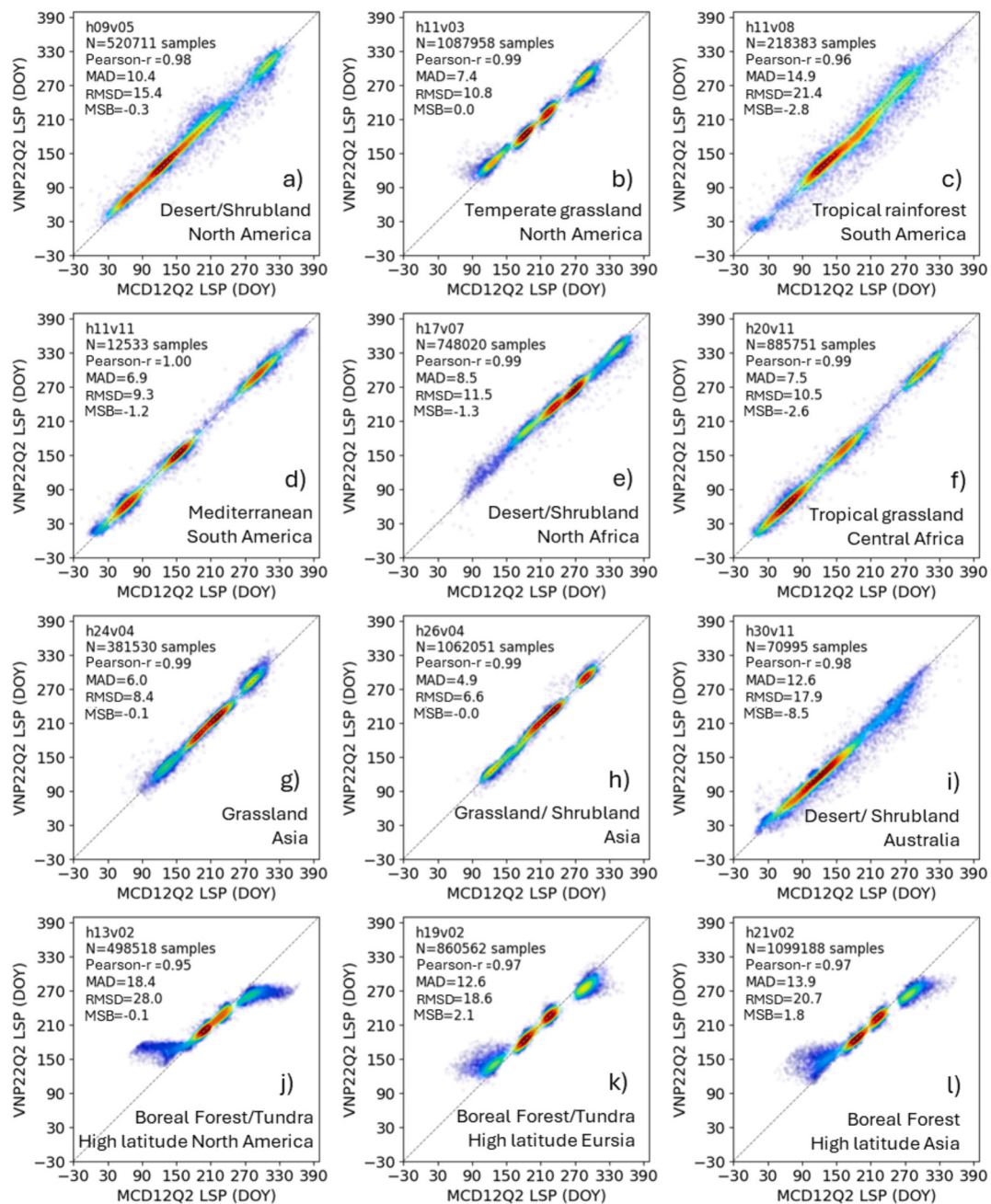


Fig. 5. Scatterplots comparing the VNP22Q2 C2 product and the MCD12Q2 C61 product in the 12 golden tiles from 2019 to 2020. Each sample corresponds to a 3×3 VIIRS pixel window with four phenological transition dates.

suggests that the LSP products derived from the VNP22Q2 C2 algorithm could provide better long-term agreement and VIIRS LSP product and consistency could be enhanced by harmonizing multiple VIIRS observations (SNPP, NOAA-20, and NOAA-21). Second, it compared phenology products, which are NASA VIIRS LSP product (VNP22Q2 C2) vs. NASA MODIS LCD product (MCD12Q2 C61), MODIS LSP product from VIIRS algorithm (MODIS-LSP) vs. MCD12Q2 C61, and VNP22Q2 C2 vs. MODIS-LSP at 500 m pixels and different land cover types across the globe. This intercomparison highlighted local geographical and ecosystem regions with agreement and discrepancy, which is essential for preserving the integrity of long-term phenological records and supporting a wide array of downstream applications, including global ecosystem modeling, environmental monitoring, agricultural forecasting, and climate variation research. Third, it explored LSP detectability with variation of EVI2 seasonality, particularly in sparsely

vegetated arid and semiarid regions where vegetation seasonality is generally subtle. It is recommended that global LSP products could be generated for the pixels with an EVI2 magnitude > 0.05 . Evidently, this study significantly extended the previous research (Zhang et al., 2018) that focused on the algorithm development for generating VIIRS LSP product based on data in the CONUS, the evaluation VIIRS LSP using field observations and Landsat phenology (both constrained by spatial mismatches and low temporal frequency), and the comparison of VIIRS LSP with MODIS phenology (generated using VIIRS algorithm) for three VIIRS tiles in the CONUS.

This study used a set of high-quality reference LSPs across North America, Europe, and Japan that fused gaps in the HLS observations with near-surface gap-free PhenoCam GCC time series for cross-evaluation of the MODIS/VIIRS phenology products. This cross-product continuity assessment significantly advanced previous

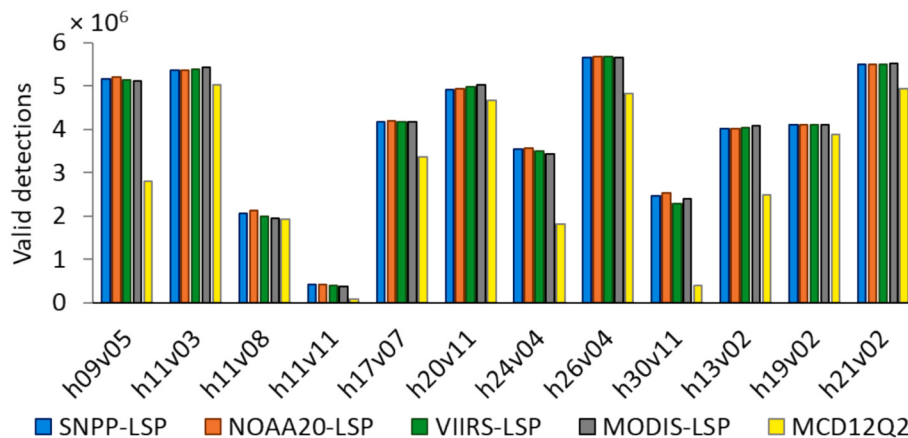


Fig. 6. The average number of valid pixels that have phenology detections for the years from 2019 to 2021 in the 12 golden tiles, generated from five 500 m LSP products: SNPP-LSP (VNP22Q2 C2), NOAA20-LSP, VIIRS2-LSP, MODIS-LSP, and MCD12Q2 C61.

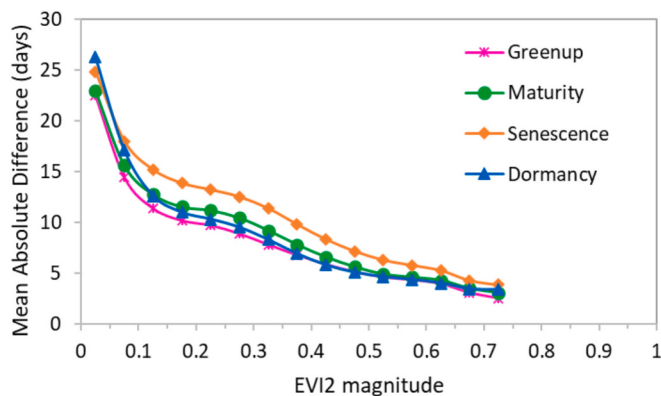


Fig. 7. The mean absolute differences (MADs) between the SNPP-LSP and NOAA20-LSP across different levels of EVI2 magnitude across all 12 golden tiles from 2019 to 2021.

assessments of MODIS and VIIRS LSP products, which used field observations, ground-based station networks, and higher spatial resolution LSP products (Bolton et al., 2020; Moon et al., 2019; Ye et al., 2022). The advance arose from the HLS-PhenoCam LSP data overcoming disadvantages in the spatial mismatch of ground observations and the large temporal gaps of higher spatial resolution time series (Tran et al., 2023a, 2023b). These intensive evaluations demonstrated that the four LSP products derived from the VNP22Q2 C2 algorithm exhibit similar uncertainties in comparison with the HLS-PhenoCam LSP product (r values = 0.98, MADs \sim 11 days, RMSDs \sim 16 days, and MSBs \sim 7 days). However, the senescence onset from the four 500 m LSP products retrieved MADs of 21–22 days and MSBs of 21–22 days relative to the HLS-PhenoCam LSP product, which indicated much larger uncertainties than the other three phenological transition dates (Table 1). These lower performances usually appeared in the east and southeast US, western US, and Spain (Fig. 4), which could be attributed to the fact that autumn phenology is more complicated than other phenological events (Rodriguez-Galiano et al., 2016; Liu et al., 2015; Xie et al., 2018).

Cross-validating the 500 m LSP products by selecting the average or median values from the 30 m phenometrics within a 3×3 MODIS or VIIRS grid can introduce uncertainties, especially in heterogeneous environments such as drylands and montane regions. Interpreting phenometrics across spatial scales remains a significant challenge, as scaling effects often distort phenological signals, although a consistent cross-scalar agreement was found using a median aggregation approach in evaluating phenometrics derived from 3 m PlanetScope, 30 m HLS, and 500 m MODIS observations (Gao et al., 2025). Biophysically, a

phenological event at the coarse scale may only become detectable once it has occurred in a certain proportion of finer-resolution pixels because multiple vegetation types with diverse phenological developments exist within that coarser pixel (Zhang et al., 2017). Thus, fine resolution phenological events could be aggregated to a coarse resolution pixel using the “percentile aggregation” approach. However, examining multi-scale phenometrics across top-of-canopy observations (Pheno-Cam), 3 m (PlanetScope), 30 m (HLS), and 450 m (VIIRS) products in dryland ecosystems, a previous study, showed that phenometric agreement across scales varied depending on surface composition (e.g., grass, shrub, bare soil), phenological stage (e.g., greenup vs. senescence), and climate conditions (normal vs. drought years), with average absolute differences ranging from 9 to 31 days (Liu et al., 2025). Similarly, this study also observed substantial discrepancies in semiarid/arid and temperate forest ecosystems (Fig. 4). Thus, it is suggested that further investigation into scale-dependent effects is necessary to better understand and mitigate uncertainties in phenological transition detection at different spatial resolutions and across various ecosystems (Shen et al., 2024; Xin et al., 2012; Zhang et al., 2017).

Results from comparisons among the five LSP products (four from the VNP22Q2 C2 algorithm and one from MCD12Q2 C61) across 12 golden tiles revealed that the LSP products derived from the VNP22Q2 C2 algorithm could provide better agreement. Overall, all these products showed good agreements among each other with r values > 0.98 , MADs \sim 4–10 days, RMSDs \sim 6–15 days, and MSBs $<$ 1 day (Table 2 and Fig. 5). Although the differences among the four products using the VNP22Q2 C2 algorithm were small (MADs $<$ 7 days), they were relatively comparable to MCD12Q2 C61 (MADs \sim 10 days). This level of similar agreement suggests that the two operational products (VNP22Q2 C2 and MCD12Q2 C61) exhibit good continuity, consistent with the earlier results from only three tiles in North America (Moon et al., 2019).

The global comparisons also showed good overall agreement in most regions. Among them, both operational products (MCD12Q2 C61 and VNP22Q2 C2) exhibited a relatively high correlation with the absolute differences of $<$ 2 weeks for most areas and LCTs (Fig. 8 and Fig. 9). Thus, the phenometrics detected from the 500 m LSP products are highly consistent across many regions around the globe despite the differences in the instruments, data processing chains, and phenological detection algorithms (Sections 1 and 2.2). Overall, the results suggest that VNP22Q2 C2 could serve as a reliable successor to the MCD12Q2 C61 record. However, the exceptions occurred at high latitudes and in semiarid regions where the four LSP products from the VNP22Q2 C2 algorithm were more comparable with one another, whereas each differed considerably from the MCD12Q2 C61 product (Figs. 8i-l). The observed global variability in Figs. 8 and 9 highlighted the spatial complexity and scale-dependent nature of phenological processes.

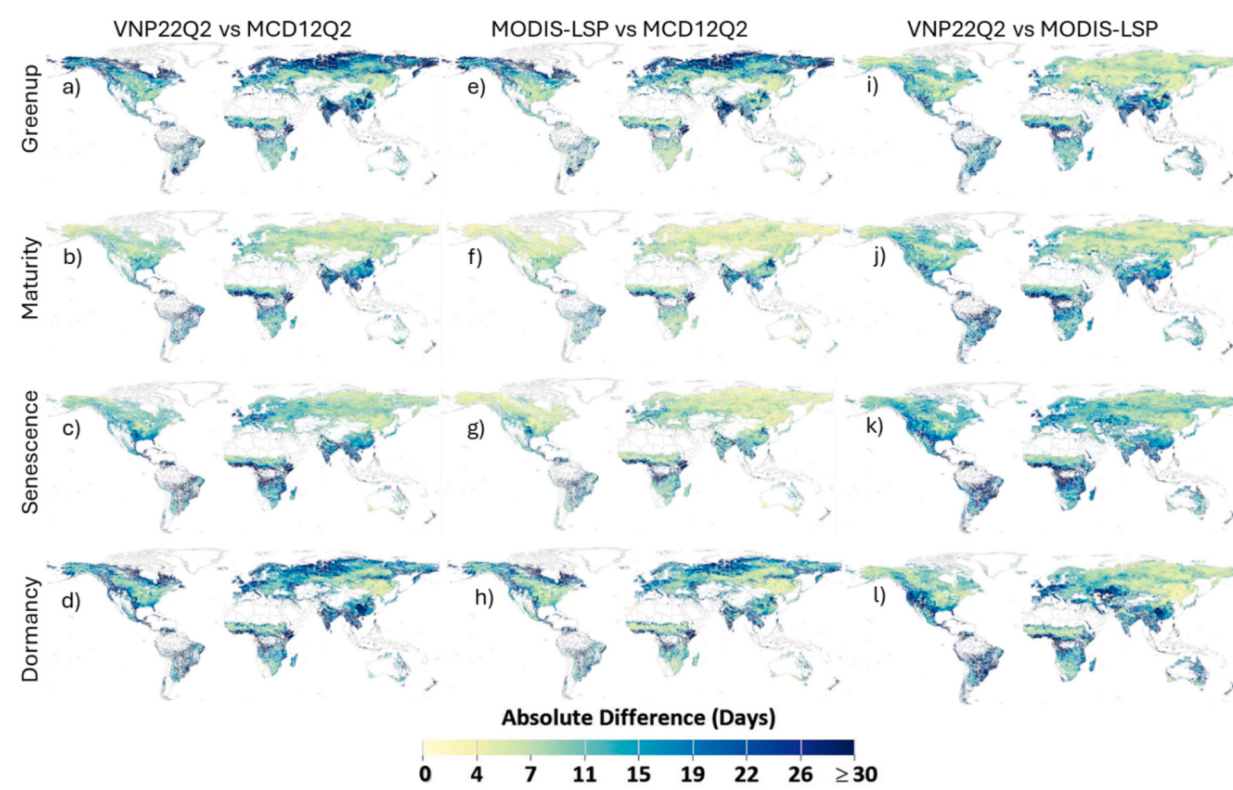


Fig. 8. Spatial patterns of the absolute differences in 2019 between the VNP22Q2 C2 and the MCD12Q2 C61 products (a – d), between MODIS-LSP and the MCD12Q2 C61 products (e – h), and between the VNP22Q2 C2 and the MODIS-LSP products (i – l).

Regional discrepancies, particularly in tropical forests, high-latitude zones, and arid/semiarid regions, could be attributed to a combination of factors, including differences in vegetation heterogeneity, phenological characteristics, climate variability, data availability (e.g., persistent cloud cover or low signal-to-noise ratios in certain biomes), and algorithm sensitivity. For example, the large MADs in evergreen broadleaf forests likely stem from persistent cloud contamination and less distinct seasonal signals, while in shrublands and arid regions, sparse vegetation cover and mixed land use could contribute to uncertainty in the timing of greenup and dormancy. Conversely, stronger agreements in temperate deciduous forests and croplands reflected more pronounced seasonal patterns and better algorithm performance in areas with regular vegetation dynamics. These findings underscore the importance of biome-specific assessments and suggest that improving LSP products may require adaptive approaches that consider regional characteristics, phenological cues, and sensor limitations.

On the other hand, all comparisons and analyses exhibited large discrepancies between MCD12Q2 C61 and VIIRS GLSP products in arid/semiarid, tropical, and high-latitude ecosystems. First, arid and semiarid ecosystems are typically characterized by very low seasonal EVI2 amplitude and are highly sensitive to irregular rainfall pulses and drought conditions (Liu et al., 2024), which leads to significant inconsistencies in phenological detections (Liu et al., 2017; Peng et al., 2021; Matthews and Mazer, 2016). The spatial patterns of MADs in the VIIRS2-LSP product comparing with the HLS-PhenoCam LSP product also showed large differences in the autumn phenology in the western US and Spain, with MADs > 25 days (Fig. 4). Thus, large discrepancies between the MCD12Q2 C61 and VIIRS GLSP products are foreseeable. Particularly, the cross-comparisons showed large differences in Australia (h30v11, as large as 13 days in MAD and 19 days in RMSD) and the western US (h09v05, as large as 10 days in MAD and 15 days in RMSD) (Table S1). The global absolute differences also displayed large differences of > 20 days in dryland areas in the western US, South

America, and some locations in Australia, Europe, and Central Asia (Fig. 8). In addition, the uncertainty investigation against the seasonality of EVI2 magnitude using the VNP22Q2 C2 algorithm over 12 golden tiles and across three years indicated that the accuracy of phenological detections substantially increased as the EVI2 magnitude increased (Fig. 7).

Based on this evidence, we suggest using a threshold of EVI2 magnitude > 0.05 in the VNP22Q2 C2 products to significantly reduce the LSP difference to < 15 days from different sensors. Alternatively, the seasonality EVI2 magnitude could be used as one of the references to determine the quality assurance of LSP detections. Furthermore, the phenological differences could arise from the sensitivity of satellite sensors to dryland vegetation. This pattern was evident that four different MODIS/VIIRS EVI2 time series commonly differ considerably, such as the example in dryland areas in South America (h11v11) from 2018 to 2020 (Fig. 10). The VIIRS SNPP obtained higher EVI2 values compared to other sensors, while the VIIRS2 (combination of SNPP and NOAA-20) time series demonstrated good agreement with the MODIS time series. These disagreements among sensors also induced large uncertainties in phenological detections among five LSP products in semiarid and arid areas (Table S1 and Fig. 8). Since phenometrics of greenness magnitude (such as seasonal minima, maxima, and rates of EVI2 change) directly influence the interpretation of seasonal vegetation dynamics and stress responses, future investigation is needed to systematically evaluate the metrics of greenness magnitude across sensors and resolutions. Such analysis would not only complement the transition-date comparisons but also enhance the ecological reliability and application readiness of LSP products under diverse environmental conditions.

Accurate and comparable detection of phenological events from different sensors is challenging in tropical areas where the number of high-quality satellite observations can be low because of persistent cloud cover and limited seasonal dynamics (e.g., evergreen broadleaf forests)

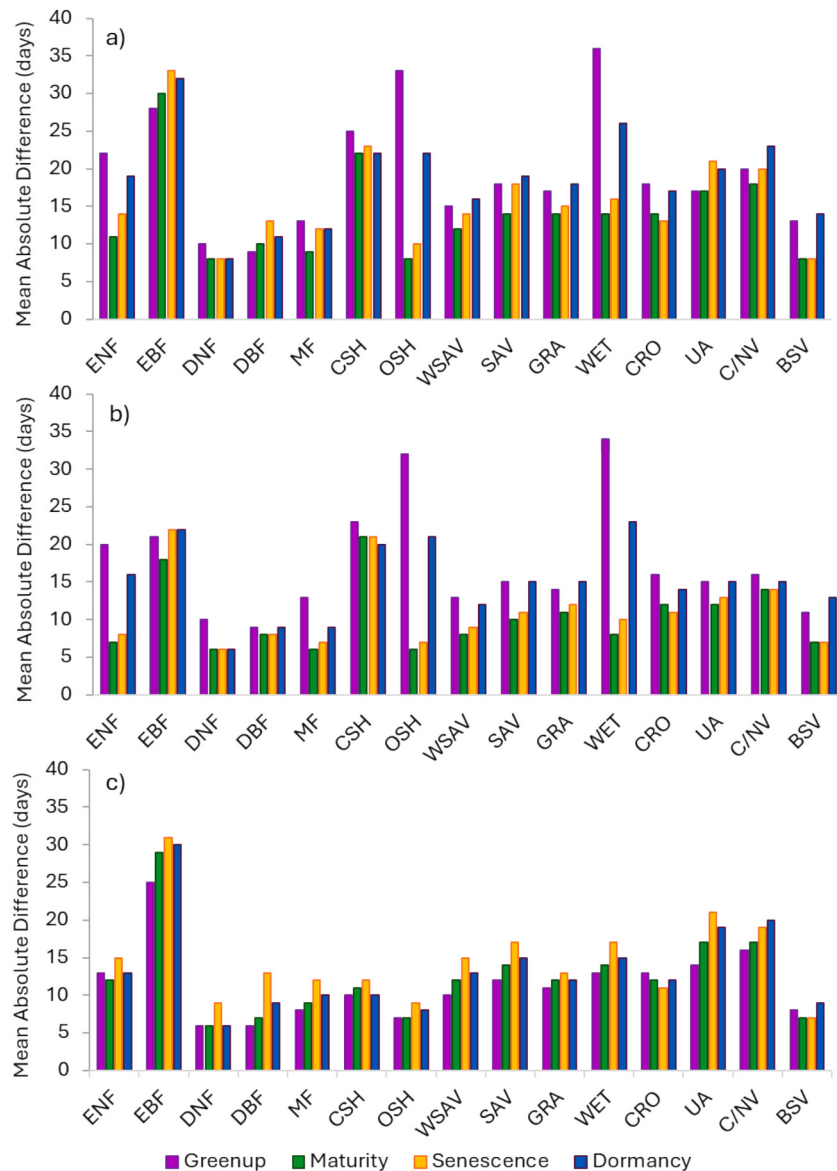


Fig. 9. The mean absolute differences (MADs) between the operational VNP22Q2 C2 and the MCD12Q2 C61 products (a), between the MODIS-LSP and MCD12Q2 C61 products (b), and between the VNP22Q2 C2 and MODIS-LSP products (c) across land cover types on four key phenological timings for the years 2019 and 2020. Land cover types acronyms decode as: ENF: evergreen needleleaf forest; EBF: evergreen broadleaf forest; DNF: deciduous needleleaf forest; DBF: deciduous broadleaf forest; MF: mixed forest; CSH: closed shrublands; OSH: open shrublands; WSAV: woody savannas; SAV: savannas; GRA: grasslands; WET: permanent wetlands; CRO: croplands; UA: urban area; C/NV: cropland/natural vegetation mosaic; BSV: barren or sparsely vegetated.

(van Schaik et al., 1993; Suepa et al., 2016; Zhang et al., 2022). Hence, similar to the arid/semiarid areas, the large discrepancies in tropical areas between the MCD12Q2 C61 and VIIRS GLSP products were not surprising. Cross-comparisons in tile h11v08 in the Amazon forest showed differences reaching 15 days in MAD and 21 days in RMSD (Table S1). Other tropical regions, such as the Congo Basin, India, and Southeast Asia, exhibited similarly large discrepancies of > 20 days (Fig. 8).

Reliable detections of LSP can be highly affected by long and snowy winter seasons in high latitudes. While the four LSP products derived from the VNP22Q2 C2 algorithm achieved very low disagreement (r values ≥ 0.99 , MADs < 6 days, RMSDs < 8 days, and MSBs < 2 days), their disagreement with the MCD12Q2 C61 product was higher with discrepancies as large as 20 days in MAD, 30 days in RMSD, and 4 days in MSB (Table S1). Notably, the greenup onset earlier than April and dormancy onset later than October detected from the MCD12Q2 C61 product in the high-latitude areas were not realistic (Fig. 5, h13v02,

h19v02, and h21v02). It is likely that the large temporal gaps due to snow cover in those high-latitude regions were inappropriately processed, which might cause significant uncertainties in the MCD12Q2 C61 product. Thus, the difference of > 25 days was found in North America, Eurasia, and Asia in the comparison between the MCD12Q2 C61 with the VNP22Q2 C2 algorithm derived products (Fig. 8). Note that the MCD12Q2 C61 algorithm utilizes snow mask from the MODIS NBAR product in an integration with Normalized Difference Snow Index (NDSI) values to determine the background EVI2 value and uses penalized cubic splines to process the time series (Gray et al., 2019), which was most likely affected by the residual or partial snow contaminations. In contrast, the VIIRS GLSP product uses the land surface temperature product in a combination to the VIIRS snow flags to eliminate snow-contaminated pixels and then fuses it with the comparable shape of EVI2 climatology (Section 2.2.1) before calculating the background value (Zhang, 2015). In other words, the VNP22Q2 C2 algorithm should be more robust in detecting phenological transitions at high

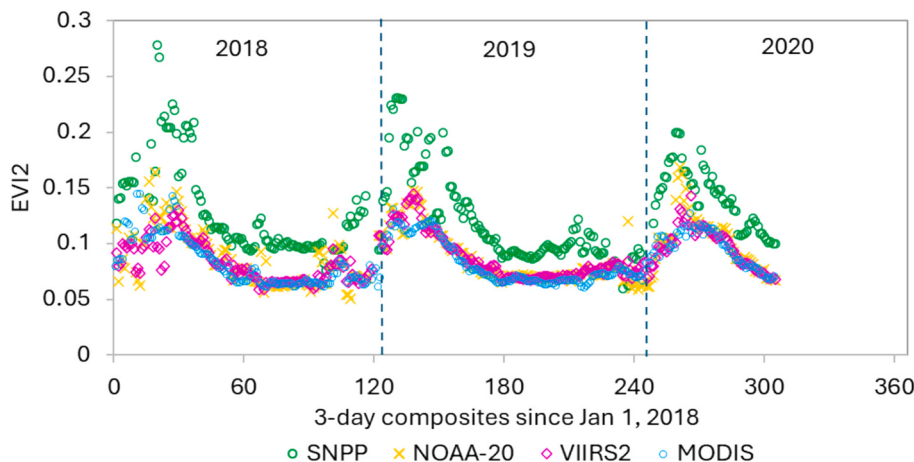


Fig. 10. Comparison of the 3-day composite two-band Enhanced Vegetation Index (EVI2) time series derived from MODIS and VIIRS sensors for a single pixel located in an arid region at 20.12°S and 66.01°W in tile h11v11 (Fig. 1). VIIRS2 denotes the combination of data from the VIIRS on both SNPP and NOAA-20 satellites.

latitudes.

The VNP22Q2 C2 algorithm could retrieve much more phenological detections than the MCD12Q2 C61 algorithm across the globe (Fig. 6 and Fig. 8), which is extremely important for various downstream applications. Technically, the MCD12Q2 C61 product detects phenometrics when the EVI2 magnitude is > 0.1 (Gray et al., 2019), while the VNP22Q2 C2 product uses a threshold of > 0.02 (Zhang et al., 2020b). The threshold of EVI2 amplitude > 0.1 could mitigate the uncertainties in LSP detections; however, this step would vastly limit the applications of the MCD12Q2 C61 product in semiarid/arid shrublands and grasslands, tropical and semitropical savannas, and evergreen forests. For instance, the MCD12Q2 C61 product only detected phenology for 26 % of Australia, where phenological information is required for various landscapes of dry, moist, and forest environments (Xie et al., 2023). Meanwhile, the VNP22Q2 C2 algorithm, with phenological detections for more pixels, significantly enhances its utility for rangelands and tropical forests monitoring and management. At the same time, as we noted above, the uncertainty in phenometrics increases as the magnitude of EVI2 amplitude decreases. Hence, the quality of phenometrics from the VNP22Q2 C2 algorithm is lower in arid and semiarid regions relative to moister ecosystems. Furthermore, a deeper exploration of the underlying causes of LSP discrepancies among sensor based products — such as those related to spectral characteristics, quality flags, and sensor-specific differences — could provide valuable insights for identifying the root causes of variability, supporting further refinement of the MCD12Q2 and VNP22Q2 algorithms, and improving its consistency and reliability of the global NASA MODIS and VIIRS phenological products for operational and research use across diverse ecosystems. We expect to reveal these underlying causes in the near future, although it is out the scope of the current study.

Harmonizing the VIIRS SNPP, NOAA-20, and NOAA-21 NBARs might improve the consistency of the EVI2 time series, which could, in turn, enhance LSP detections. Large temporal gaps could significantly reduce the quality of the satellite time series for phenological detections and introduce substantial uncertainties in LSP products (Bolton et al., 2020; Zhang et al., 2020a; Tran et al., 2025). Currently, both MODIS Terra (10:30 AM) and Aqua (1:30 PM) platforms are used for the generation of the MCD12Q2 C61 product, offering synergistic advantages that increase the chances of capturing cloud-free observations throughout the growing season of vegetation (Moon et al., 2019). Whereas VIIRS GLSP product primarily uses the SNPP (1:30 PM) observations (Zhang et al., 2020b). The improvement of the LSP detections from SNPP and NOAA-20 data was evident (cf. Table 3). The average agreement of each LSP product with four other LSP products in 12 golden tiles showed that the VIIRS2-LSP (combining VIIRS SNPP and NOAA-20 NBAR) exhibited the

Table 3

The average agreement of each LSP product with four other LSP products in the 12 golden tiles from 2019 to 2021, which is calculated from Table 2.

	SNPP-LSP	NOAA-LSP	VIIRS2-LSP	MODIS-LSP	MCD12Q2
r	0.99	0.99	0.99	0.99	0.98
MAD	7.1	6.8	6.3	7.0	10.0
RMSD	10.2	9.8	9.1	10.0	14.7
MSB	-0.6	-0.3	-0.4	-0.5	-0.6

lowest discrepancies among five LSP products with 1–4 days smaller in MADs and 1–5 days smaller in RMSDs. For instance, the VIIRS2-LSP achieved MADs ~ 11 days and RMSDs ~ 16 days in the tropical areas in the Amazon forest (h11v08), which were 2–3 days smaller than other LSP products (Table S1). This finding was likely due to the VIIRS2 EVI2 time series being more consistent with the MODIS time series for better phenological detections in drylands (Fig. 10). The better performances from the VIIRS2-LSP were 2–3 days smaller in h09v05 (western US), h11v11 (South America), and h30v11 (Australia) (Table S1). Thus, integrating SNPP, NOAA-20, and potentially NOAA-21 could create a higher-quality VIIRS time series for producing a unified VIIRS GLSP product with enhanced accuracy and reliability.

Furthermore, the VNP22Q2 C2 algorithm could be implemented on the MODIS NBAR time series to significantly enhance the continuous measurement of the long-term global phenology data records. Note that the MODIS-LSP was more consistent with the VIIRS LSP products than the MCD12Q2 C61 product in the following aspects. First, the MODIS-LSP was able to decrease MAD from 19 days to 4 days and RMSD from 29 days to 6 days at high latitudes (Table S1, h13v02, h19v02, and h21v02). Second, compared with the VNP22Q2 C2, the MODIS-LSP could reduce two to five days of discrepancies in tropical Amazon forest (h11v08) and drylands (h09v05 and h30v11) than the operational MCD12Q2 C61 product (Table S1). Third, similar to the VNP22Q2 C2 product, the MODIS-LSP was able to produce more valid phenology detections across drylands, which was a clear limitation in the MCD12Q2 C61 product (Fig. 6 and Fig. 8).

Finally, a recent independent comparison of VNP22Q2 C2 and MCD12Q2 C61 products, which focused on the mid-greenup phenometric assessed across global ecoregions, found significant inconsistencies, especially in ecoregions with reduced seasonal amplitudes or varied seasonality, and in ecoregions close to water, such as mangroves (de Beurs et al., 2025). They found the mid-greenup phenometrics well-aligned for ecoregions in temperate and colder biomes, but not for moist and dry biomes. Moreover, the phenological detections were stable and robust primarily observed in temperate ecoregions

characterized by unimodal seasonality (de Beurs et al., 2025).

In summary, this study provides significant new results and methods that advance the science and global application of land surface phenology products in multiple ways. First, applying spatially scalable references of phenological data from the fusion between HLS and PhenoCam for evaluating phenology products overcame a prior disadvantage in the spatial mismatch of ground observations and the large temporal gaps of higher spatial resolution time series. Second, investigating the algorithm in detecting phenology from a single VIIRS sensor and from multiple VIIRS sensors offered an approach to generate future global phenology product using multiple streams of VIIRS observations, namely from Suomi NPP (launched 2011), NOAA-20 (launched 2017), NOAA-21 (launched 2022), NOAA-22 (scheduled for 2027), and NOAA-23 (scheduled for 2032). Third, analyzing the phenological discrepancies between two products against greenness magnitudes advanced our knowledge of phenology detectability in drylands, an area needing improvement in future phenology products. Finally, the new results of the similarities and discrepancies between VNP22Q2 C2 and MCD12Q2 C61 products across global regions may significantly advance scientific investigations into long-term ecosystem functioning and climate system feedbacks.

5. Conclusions

A high-quality long-term record of GLSP products is important for downstream applications, including global modeling, ecological and environmental monitoring, and climate change research. Therefore, this study conducted complementary analyses and quantitative evaluations globally of discrepancies among MODIS LCD and VIIRS GLSP products at 500 m spatial resolution. We first cross-evaluated the MODIS/VIIRS LSP products in 2019 and 2020 using a high-quality reference of the HLS-PhenoCam LSP product at 30 m across North America, Europe, and Japan. The results showed the four LSP products derived from the VNP22Q2 C2 algorithm (SNPP-LSP, NOAA20-LSP, VIIRS2-LSP, MODIS-LSP) consistently obtained comparable accuracy with r values = 0.98, MADs \sim 11 days, RMSDs \sim 16 days, and MSBs \sim 7 days. The cross-comparisons among the five 500 m LSP products across 12 golden tiles indicated the VNP22Q2 C2 algorithm based products exhibited very high agreement, with MADs $<$ 7 days, RMSDs $<$ 10 days, and MSBs $<$ 1 day, whereas their correlations with the MCD12Q2 C61 could be three days and five days larger in MAD and RMSD, respectively. Finally, comparisons between the operational MCD12Q2 C61 and VNP22Q2 C2 products across the globe revealed that the VNP22Q2 C2 product could provide great global continuity with the MCD12Q2 C61 record with an absolute difference of $<$ 15 days for most of the areas across the globe, except for the arid/semiarid, tropical, and high-latitude ecosystems. However, the VNP22Q2 C2 algorithm performed better than the MCD12Q2 C61 algorithm in terms of producing phenological detections for more pixels and detecting accurate phenological events at high latitudes. Based on all the analyses, we provide two suggestions for the next steps to ensure continuity. First, integrate all VIIRS data streams from SNPP, NOAA-20, and NOAA-21 to generate a single VIIRS time series synthetic of higher quality for producing a more robust VIIRS GLSP product. Second, apply the VIIRS phenological detection algorithm to the MODIS time series to further enhance the global continuity of the long-term phenological measurement records.

CRediT authorship contribution statement

Khuong H. Tran: Writing – review & editing, Writing – original draft, Visualization, Validation, Software, Resources, Project administration, Methodology, Investigation, Formal analysis, Data curation, Conceptualization. **Xiaoyang Zhang:** Writing – review & editing, Writing – original draft, Supervision, Methodology, Funding acquisition, Conceptualization. **Yongchang Ye:** Writing – review & editing, Software, Resources, Data curation. **Geoffrey M. Henebry:** Writing – review

& editing, Conceptualization. **Mark A. Friedl:** Writing – review & editing, Conceptualization. **Yu Shen:** Writing – review & editing. **Yuxia Liu:** Writing – review & editing. **Shuai An:** Writing – review & editing. **Shuai Gao:** Writing – review & editing.

Declaration of competing interest

The authors declare that they have no known competing financial interests or personal relationships that could have appeared to influence the work reported in this paper.

Data availability

I have shared link of data in the paper

Acknowledgements

This work was supported by NASA grants 80NSSC18K0626 and 80NSSC21K1962. We also acknowledge the NASA Earth Exchange for partial support of this project. We further thank the NASA Oak Ridge National Laboratory DAAC (ORNL DAAC) for providing the HLS-PhenoCam LSP product and the Earth Science Data Systems (ESDS) Program for providing the MODIS Land Cover Dynamics (MCD12Q2) and VIIRS Land Surface Phenology (VNP22Q2). Finally, we thank the two anonymous reviewers and the editors whose comments, questions, and suggestions helped us to improve the clarity, precision, and relevance of our manuscript.

Appendix A. Supplementary data

Supplementary data to this article can be found online at <https://doi.org/10.1016/j.rse.2025.115024>.

References

- Adole, T., Dash, J., Atkinson, P.M., 2016. A systematic review of vegetation phenology in Africa. *Ecol. Inform.* 34, 117–128. <https://doi.org/10.1016/J.ECOINF.2016.05.004>.
- de Almeida, C.A., Coutinho, A.C., Esquerdo, J.C., Dalla, M., Adami, M., Venturieri, A., Diniz, C.G., Dessay, N., Durieux, L., Gomes, A.R., 2016. High spatial resolution land use and land cover mapping of the Brazilian legal Amazon in 2008 using Landsat-5/TM and MODIS data. *Acta Amazon.* 46, 291–302. <https://doi.org/10.1590/1809-4392201505504>.
- Berra, E.F., Gaulton, R., 2021. Remote sensing of temperate and boreal forest phenology: a review of progress, challenges and opportunities in the intercomparison of in-situ and satellite phenological metrics. *For. Ecol. Manage.* 480, 118663. <https://doi.org/10.1016/j.foreco.2020.118663>.
- de Beurs, K.M., Henebry, G.M., 2008. Northern annular mode effects on the land surface phenologies of northern Eurasia. *J. Climate* 21 (17), 4257–4279. <https://doi.org/10.1175/2008JCLI2074.1>.
- de Beurs, K.M., Driscoll, E., Henebry, G.M., 2025. Land surface phenology in global change studies. In: Schwartz, M.D. (Ed.), *Phenology: An Integrative Environmental Science*, 3rd edition. Springer, Cham, pp. 505–529. https://doi.org/10.1007/978-3-031-75027-4_22.
- Bolton, D.K., Gray, J.M., Melaas, E.K., Moon, M., Eklundh, L., Friedl, M.A., 2020. Continental-scale land surface phenology from harmonized Landsat 8 and Sentinel-2 imagery. *Remote Sens. Environ.* 240, 111685. <https://doi.org/10.1016/j.rse.2020.111685>.
- Brown, T.B., Hultine, K.R., Steltzer, H., Denny, E.G., Denslow, M.W., Granados, J., Henderson, S., Moore, D., Nagai, S., SanClementes, M., Sánchez-Azofeifa, A., Sonnentag, O., Tazik, D., Richardson, A.D., 2016. Using phenocams to monitor our changing earth: toward a global phenocam network. *Front. Ecol. Environ.* 14, 84–93. <https://doi.org/10.1002/fee.1222>.
- Chen, S., Fu, Y.H., Hao, F., Li, X., Zhou, S., Liu, C., Tang, J., 2022. Vegetation phenology and its ecohydrological implications from individual to global scales. *Geogr. Sustainability* 3, 334–338. <https://doi.org/10.1016/J.GEOSUS.2022.10.002>.
- Cleland, E.E., Allen, J.M., Crimmins, T.M., Dunne, J.A., Pau, S., Travers, S.E., Zavaleta, E.S., Wolkovich, E.M., 2012. Phenological tracking enables positive species responses to climate change. *Ecology* 93, 1765–1771. <https://doi.org/10.1890/11-1912.1>.
- Friedl, M.A., McIver, D.K., Hodges, J.C.F., Zhang, X.Y., Muchoney, D., Strahler, A.H., Woodcock, C.E., Gopal, S., Schneider, A., Cooper, A., Baccini, A., Gao, F., Schaaf, C., 2002. Global land cover mapping from MODIS: algorithms and early results. *Remote Sens. Environ.* 83, 287–302. [https://doi.org/10.1016/S0034-4257\(02\)00078-0](https://doi.org/10.1016/S0034-4257(02)00078-0).
- Friedl, M.A., Sulla-Menashe, D., Tan, B., Schneider, A., Ramankutty, N., Sibley, A., Huang, X., 2010. MODIS collection 5 global land cover: algorithm refinements and

- characterization of new datasets. *Remote Sens. Environ.* 114, 168–182. <https://doi.org/10.1016/J.RSE.2009.08.016>.
- Friedl, M.A., Gray, J.M., Melaas, E.K., Richardson, A.D., Hufkens, K., Keenan, T.F., Bailey, A., O'Keefe, J., 2014. A tale of two springs: using recent climate anomalies to characterize the sensitivity of temperate forest phenology to climate change. *Environ. Res. Lett.* 9, 54006. <https://doi.org/10.1088/1748-9326/9/5/054006>.
- Ganguly, S., Friedl, M.A., Tan, B., Zhang, X., Verma, M., 2010. Land surface phenology from MODIS: characterization of the collection 5 global land cover dynamics product. *Remote Sens. Environ.* 114, 1805–1816. <https://doi.org/10.1016/j.rse.2010.04.005>.
- Gao, X., Stonebrook, S., Green, T., Moon, M., Friedl, M.A., 2025. Cross-scalar analysis of multisensor land surface phenology. *Remote Sens. Environ.* 319, 114624.
- Gray, J., Sulla-Menashe, D., Friedl, M.A., 2019. User Guide to Collection 6 Modis Land Cover Dynamics (mcd12q2) Product. NASA EOSDIS Land Processes DAAC: Missoula, MT, USA.
- Gutman, G.G., 1999. On the use of long-term global data of land reflectances and vegetation indices derived from the advanced very high resolution radiometer. *J. Geophys. Res. Atmos.* 104, 6241–6255. <https://doi.org/10.1029/1998JD200106>.
- Henebry, G.M., de Beurs, K.M., 2025. Remote sensing of land surface phenology: Progress, challenges, prospects. In: *Phenology: An Integrative Environmental Science*, 3rd edition. Springer Nature Switzerland, Cham, pp. 431–459. https://doi.org/10.1007/978-3-031-75027-4_19.
- Julien, Y., Sobrino, J.A., 2009. Global land surface phenology trends from GIMMS database. *Int. J. Remote Sens.* 30, 3495–3513. <https://doi.org/10.1080/01431160802562255>.
- Justice, C.O., Townshend, J.R.G., Holben, B.N., Tucker, C.J., 1985. Analysis of the phenology of global vegetation using meteorological satellite data. *Int. J. Remote Sens.* 6, 1271–1318. <https://doi.org/10.1080/01431168509848281>.
- Justice, C.O., Román, M.O., Csizsar, I., Vermote, E.F., Wolfe, R.E., Hook, S.J., Friedl, M., Wang, Z., Schaaf, C.B., Miura, T., Tschudi, M., Riggs, G., Hall, D.K., Lyapustin, A.I., Devadiga, S., Davidson, C., Masuoka, E.J., 2013. Land and cryosphere products from Suomi NPP VIIRS: overview and status. *J. Geophys. Res. Atmos.* 118, 9753–9765. <https://doi.org/10.1002/JGRD.50771>.
- Klosterman, S.T., Hufkens, K., Gray, J.M., Melaas, E., Sonnentag, O., Lavine, I., Mitchell, L., Norman, R., Friedl, M.A., Richardson, A.D., 2014. Evaluating remote sensing of deciduous forest phenology at multiple spatial scales using PhenoCam imagery. *Biogeosciences* 11, 4305–4320. <https://doi.org/10.5194/bg-11-4305-2014>.
- Li, X., Zhou, Y., Asrar, G.R., Meng, L., 2017. Characterizing spatiotemporal dynamics in phenology of urban ecosystems based on Landsat data. *Sci. Total Environ.* 605–606, 721–734. <https://doi.org/10.1016/j.scitotenv.2017.06.245>.
- Liu, Lingling, Liang, L., Schwartz, M.D., Donnelly, A., Wang, Z., Schaaf, C.B., Liu, Liangyun, 2015. Evaluating the potential of MODIS satellite data to track temporal dynamics of autumn phenology in a temperate mixed forest. *Remote Sens. Environ.* 160, 156–165. <https://doi.org/10.1016/J.RSE.2015.01.011>.
- Liu, Y., Hill, M.J., Zhang, X., Wang, Z., Richardson, A.D., Hufkens, K., Filippa, G., Baldocchi, D.D., Ma, S., Verfaillie, J., Schaaf, C.B., 2017. Using data from Landsat, MODIS, VIIRS and PhenoCams to monitor the phenology of California oak/grass savanna and open grassland across spatial scales. *Agric. For. Meteorol.* 237–238, 311–325. <https://doi.org/10.1016/j.agrformet.2017.02.026>.
- Liu, Y., Zhang, X., Shen, Y., Ye, Y., Gao, S., Tran, K.H., 2024. Evaluation of PlanetScope-detected plant-specific phenology using infrared-enabled PhenoCam observations in semi-arid ecosystems. *ISPRS J. Photogram. Rem. Sens.* 210, 242–259. <https://doi.org/10.1016/J.ISPRSJPRS.2024.03.017>.
- Liu, Y., Zhang, X., Tran, K.H., Ye, Y., Shen, Y., An, S., 2025. Heterogeneous land surface phenology challenges the comparison among PlanetScope, HLS, and VIIRS detections in semi-arid rangelands. *Agric. For. Meteorol.* 366, 110497.
- Loveland, T.R., Belward, A.S., 1997. The international geosphere biosphere Programme data and information system: global land cover data set (DISCover). *Acta Astronaut.* 41, 681–689. [https://doi.org/10.1016/S0094-5765\(98\)00050-2](https://doi.org/10.1016/S0094-5765(98)00050-2).
- Lyapustin, A., Wang, Y., Choi, M., Xiong, X., Angal, A., Wu, A., Doelling, D.R., Bhatt, R., Go, S., Korkin, S., Franz, B., Meister, G., Sayer, A.M., Roman, M., Holz, R.E., Meyer, K., Gleason, J., Levy, R., 2023. Calibration of the SNPP and NOAA 2 VIIRS sensors for continuity of the MODIS climate data records. *Remote Sens. Environ.* 295, 113717. <https://doi.org/10.1016/J.RSE.2023.113717>.
- Matthews, E.R., Mazer, S.J., 2016. Historical changes in flowering phenology are governed by temperature × precipitation interactions in a widespread perennial herb in western North America. *New Phytol.* 210, 157–167. <https://doi.org/10.1111/NPH.13751>.
- Melaas, E.K., Sulla-Menashe, D., Friedl, M.A., 2018. Multidecadal changes and interannual variation in springtime phenology of north American temperate and boreal deciduous forests. *Geophys. Res. Lett.* 45, 2679–2687. <https://doi.org/10.1002/2017GL076933>.
- Moon, M., Zhang, X., Henebry, G.M., Liu, L., Gray, J.M., Melaas, E.K., Friedl, M.A., 2019. Long-term continuity in land surface phenology measurements: a comparative assessment of the MODIS land cover dynamics and VIIRS land surface phenology products. *Remote Sens. Environ.* 226, 74–92. <https://doi.org/10.1016/j.rse.2019.03.034>.
- Morissette, J.T., Richardson, A.D., Knapp, A.K., Fisher, J.I., Graham, E.A., Abatzoglou, J., Wilson, B.E., Breshears, D.D., Henebry, G.M., Hanes, J.M., Liang, L., 2009. Tracking the rhythm of the seasons in the face of global change: phenological research in the 21st century. *Front. Ecol. Environ.* 7, 253–260. <https://doi.org/10.1890/070217>.
- Mu, Q., Zhao, M., Running, S.W., 2011. Improvements to a MODIS global terrestrial evapotranspiration algorithm. *Remote Sens. Environ.* 115, 1781–1800. <https://doi.org/10.1016/J.RSE.2011.02.019>.
- Nagol, J.R., Vermote, E.F., Prince, S.D., 2009. Effects of atmospheric variation on AVHRR NDVI data. *Remote Sens. Environ.* 113, 392–397. <https://doi.org/10.1016/J.RSE.2008.10.007>.
- Peng, D., Wang, Y., Xian, G., Huete, A.R., Huang, W., Shen, M., Wang, F., Yu, L., Liu, Liangyun, Xie, Q., Liu, Lingling, Zhang, X., 2021. Investigation of land surface phenology detections in shrublands using multiple scale satellite data. *Remote Sens. Environ.* 252, 112133. <https://doi.org/10.1016/J.RSE.2020.112133>.
- Pérez-Hoyos, A., Rembold, F., Kerdiles, H., Gallego, J., 2017. Comparison of global land cover datasets for cropland monitoring. *Rem. Sens.* Vol. 9, page 1118. doi:<https://doi.org/10.3390/RS9111118>.
- Richardson, A.D., 2023. PhenoCam: An evolving, open-source tool to study the temporal and spatial variability of ecosystem-scale phenology. *Agric. For. Meteorol.* 342, 109751. <https://doi.org/10.1016/J.JAGRFORMAT.2023.109751>.
- Richardson, A.D., Keenan, T.F., Migliavacca, M., Ryu, Y., Sonnentag, O., Toomey, M., 2013. Climate change, phenology, and phenological control of vegetation feedbacks to the climate system. *Agric. For. Meteorol.* 169, 156–173. <https://doi.org/10.1016/J.JAGRFORMAT.2012.09.012>.
- Rodriguez-Galiano, V.F., Sanchez-Castillo, M., Dash, J., Atkinson, P.M., Ojeda-Zujar, J., 2016. Modelling interannual variation in the spring and autumn land surface phenology of the European forest. *Biogeosciences* 13, 3305–3317. <https://doi.org/10.5194/BG-13-3305-2016>.
- Román, M.O., Justice, C., Paynter, I., Boucher, P.B., Devadiga, S., Endsley, A., Erb, A., Friedl, M., Gao, H., Giglio, L., Gray, J.M., Hall, D., Hulley, G., Kimball, J., Knyazikhin, Y., Lyapustin, A., Myneni, R.B., Noojipady, P., Pu, J., Riggs, G., Sarkar, S., Schaaf, C., Shah, D., Tran, K.H., Vermote, E., Wang, D., Wang, Z., Wu, A., Ye, Y., Shen, Y., Zhang, S., Zhang, X., Zhao, M., Davidson, C., Wolfe, R., 2024. Continuity between NASA MODIS collection 6.1 and VIIRS collection 2 land products. *Remote Sens. Environ.* 302, 113963. <https://doi.org/10.1016/J.RSE.2023.113963>.
- van Schaik, C.P., Terborgh, J.W., Wright, S.J., 1993. The phenology of tropical forests: adaptive significance and consequences for primary consumers. *Annu. Rev. Ecol. Syst.* 24, 353–377.
- Shen, Y., Zhang, X., Wang, W., Nemani, R., Ye, Y., Wang, J., 2021. Fusing geostationary satellite observations with harmonized Landsat-8 and Sentinel-2 time series for monitoring field-scale land surface phenology. *Remote Sens. (Basel)* 13. <https://doi.org/10.3390/rs13214465>.
- Shen, Y., Zhang, X., Gao, S., Zhang, H.K., Schaaf, C., Wang, W., Ye, Y., Liu, Y., Tran, K.H., 2024. Analyzing GOES-R ABI BRDF-adjusted EVI2 time series by comparing with VIIRS observations over the CONUS. *Remote Sens. Environ.* 302, 113972. <https://doi.org/10.1016/J.RSE.2023.113972>.
- Stucky, B.J., Guralnick, R., Deck, J., Denny, E.G., Bolmgren, K., Walls, R., 2018. The plant phenology ontology: a new informatics resource for large-scale integration of plant phenology data. *Front. Plant Sci.* 9. <https://doi.org/10.3389/fpls.2018.00517>.
- Suepa, T., Qi, J., Lawawirojwong, S., Messina, J.P., 2016. Understanding spatio-temporal variation of vegetation phenology and rainfall seasonality in the monsoon Southeast Asia. *Environ. Res.* 147, 621–629. <https://doi.org/10.1016/J.ENVR.2016.02.005>.
- Sulla-Menashe, D., Woodcock, C.E., Friedl, M.A., 2018. Canadian boreal forest greening and browning trends: an analysis of biogeographic patterns and the relative roles of disturbance versus climate drivers. *Environ. Res. Lett.* 13, 014007. <https://doi.org/10.1088/1748-9326/AA9B88>.
- Tran, K.H., Zhang, X., Ketchpaw, A.R., Wang, J., Ye, Y., Shen, Y., 2022. A novel algorithm for the generation of gap-free time series by fusing harmonized Landsat 8 and Sentinel-2 observations with PhenoCam time series for detecting land surface phenology. *Remote Sens. Environ.* 282, 113275. <https://doi.org/10.1016/j.rse.2022.113275>.
- Tran, K.H., Zhang, X., Ye, Y., Shen, Y., Gao, S., Liu, Y., Richardson, A., 2023a. HP-LSP: a reference of land surface phenology from fused harmonized Landsat and Sentinel-2 with PhenoCam data. *Sci. Data* 10, 691. <https://doi.org/10.1038/s41597-023-02605-1>.
- Tran, K.H., Zhang, X., Ye, Y., Shen, Y., Gao, S., Liu, Y., Richardson, A.D., 2023b. Phenology Derived from Satellite Data and PhenoCam across CONUS and Alaska, 2019–2020. <https://doi.org/10.3334/ORNLDAA/C2248>.
- Tran, K.H., Zhang, X., Zhang, H.K., Shen, Y., Ye, Y., Liu, Y., Gao, S., An, S., 2025. A transformer-based model for detecting land surface phenology from the irregular harmonized Landsat and Sentinel-2 time series across the United States. *Remote Sens. Environ.* 320, 114656. <https://doi.org/10.1016/j.rse.2025.114656>.
- Vrieling, A., Skidmore, A.K., Wang, T., Meroni, M., Ens, B.J., Oosterbeek, K., O'Connor, B., Darvishzadeh, R., Heurich, M., Shepherd, A., Paganini, M., 2017. Spatially detailed retrievals of spring phenology from single-season high-resolution image time series. *Int. J. Appl. Earth Observat. Geoinform.* 59, 19–30. <https://doi.org/10.1016/j.jag.2017.02.021>.
- Wan, Z., 2008. New refinements and validation of the MODIS land-surface temperature/emissivity products. *Remote Sens. Environ.* 112, 59–74. <https://doi.org/10.1016/J.RSE.2006.06.026>.
- White, M.A., de Beurs, K.M., Didan, K., Inouye, D.W., Richardson, A.D., Jensen, O.P., O'Keefe, J., Zhang, G., Nemani, R.R., van Leeuwen, W.J.D., Brown, J.F., de Wit, A., Schaepman, M., Lin, X., Dettinger, M., Bailey, A.S., Kimball, J., Schwartz, M.D., Baldocchi, D.D., Lee, J.T., Lauenroth, W.K., 2009. Intercomparison, interpretation, and assessment of spring phenology in North America estimated from remote sensing for 1982–2006. *Glob. Chang. Biol.* 15, 2335–2359. <https://doi.org/10.1111/J.1365-2486.2009.01910.X>.
- Wu, C., Wang, J., Caias, P., Peñuelas, J., Zhang, X., Sonnentag, O., Tian, F., Wang, X., Wang, H., Liu, R., Fu, Y.H., Ge, Q., 2021. Widespread decline in winds delayed autumn foliar senescence over high latitudes. *Proc. Natl. Acad. Sci. U. S. A.* 118, e2015821118. https://doi.org/10.1073/PNAS.2015821118/SUPPL_FILE/PNAS.2015821118.SAPP.PDF.

- Xie, Q., Moore, C.E., Cleverly, J., Hall, C.C., Ding, Y., Ma, X., Leigh, A., Huete, A., 2023. Land surface phenology indicators retrieved across diverse ecosystems using a modified threshold algorithm. *Ecol. Indic.* 147, 110000. <https://doi.org/10.1016/J.ECOLIND.2023.110000>.
- Xie, Y., Wang, X., Wilson, A.M., Silander, J.A., 2018. Predicting autumn phenology: how deciduous tree species respond to weather stressors. *Agric. For. Meteorol.* 250–251, 127–137. <https://doi.org/10.1016/J.AGRFORMAT.2017.12.259>.
- Xin, Q., Woodcock, C.E., Liu, J., Tan, B., Melloh, R.A., Davis, R.E., 2012. View angle effects on MODIS snow mapping in forests. *Remote Sens. Environ.* 118, 50–59. <https://doi.org/10.1016/J.RSE.2011.10.029>.
- Yan, K., Park, T., Yan, G., Chen, C., Yang, B., Liu, Z., Nemani, R.R., Knyazikhin, Y., Myneni, R.B., 2016. Evaluation of MODIS LAI/FPAR product collection 6. Part 1: consistency and improvements. *Rem. Sens.*, Vol. 8, page 359. doi:<https://doi.org/10.3390/RS8050359>.
- Ye, Y., Zhang, X., Shen, Y., Wang, J., Crimmins, T., Scheifinger, H., 2022. An optimal method for validating satellite-derived land surface phenology using in-situ observations from national phenology networks. *ISPRS J. Photogramm. Remote Sens.* 194, 74–90. <https://doi.org/10.1016/J.ISPRSJPRS.2022.09.018>.
- Zhang, H.K., Roy, D.P., 2017. Using the 500 m MODIS land cover product to derive a consistent continental scale 30 m Landsat land cover classification. *Remote Sens. Environ.* 197, 15–34. <https://doi.org/10.1016/j.rse.2017.05.024>.
- Zhang, X., 2015. Reconstruction of a complete global time series of daily vegetation index trajectory from long-term AVHRR data. *Remote Sens. Environ.* 156, 457–472. <https://doi.org/10.1016/j.rse.2014.10.012>.
- Zhang, X., Friedl, M.A., Schaaf, C.B., Strahler, A.H., Hodges, J.C.F., Gao, F., Reed, B.C., Huete, A., 2003. Monitoring vegetation phenology using MODIS. *Remote Sens. Environ.* 84, 471–475. [https://doi.org/10.1016/S0034-4257\(02\)00135-9](https://doi.org/10.1016/S0034-4257(02)00135-9).
- Zhang, X., Friedl, M.A., Schaaf, C.B., 2006. Global vegetation phenology from moderate resolution imaging Spectroradiometer (MODIS): evaluation of global patterns and comparison with in situ measurements. *J. Geophys. Res. Biogeosci.* 111. <https://doi.org/10.1029/2006JG000217>.
- Zhang, X., Friedl, M.A., Schaaf, C.B., 2009. Sensitivity of vegetation phenology detection to the temporal resolution of satellite data. *Int. J. Rem. Sens.* 30, 2061–2074. <https://doi.org/10.1080/01431160802549237>.
- Zhang, X., Wang, J., Gao, F., Liu, Y., Schaaf, C., Friedl, M., Yu, Y., Jayavelu, S., Gray, J., Liu, L., Yan, D., Henebry, G.M., 2017. Exploration of scaling effects on coarse resolution land surface phenology. *Remote Sens. Environ.* 190, 318–330. <https://doi.org/10.1016/j.rse.2017.01.001>.
- Zhang, X., Liu, L., Liu, Y., Jayavelu, S., Wang, J., Moon, M., Henebry, G.M., Friedl, M.A., Schaaf, C.B., 2018. Generation and evaluation of the VIIRS land surface phenology product. *Remote Sens. Environ.* 216, 212–229. <https://doi.org/10.1016/j.rse.2018.06.047>.
- Zhang, X., Wang, J., Henebry, G.M., Gao, F., 2020a. Development and evaluation of a new algorithm for detecting 30 m land surface phenology from VIIRS and HLS time series. *ISPRS J. Photogramm. Rem. Sens.* 161, 37–51. <https://doi.org/10.1016/j.isprsjprs.2020.01.012>.
- Zhang, X., Wang, J., Ye, Y., 2020b. Development of global land surface phenology product from time series of VIIRS observations. In: IGARSS 2020–2020 IEEE International Geoscience and Remote Sensing Symposium. IEEE, pp. 4795–4798. <https://doi.org/10.1109/IGARSS39084.2020.9324392>.
- Zhang, X., Gao, F., Wang, J., Ye, Y., 2021. Evaluating a spatiotemporal shape-matching model for the generation of synthetic high spatiotemporal resolution time series of multiple satellite data. *Int. J. Appl. Earth Obs. Geoinf.* 104, 102545. <https://doi.org/10.1016/j.jag.2021.102545>.
- Zhang, X., Shen, Y., Gao, S., Wang, W., Schaaf, C., 2022. Diverse responses of multiple satellite-derived vegetation Greenup onsets to dry periods in the Amazon. *Geophys. Res. Lett.* 49, e2022GL098662. <https://doi.org/10.1029/2022GL098662>.